Probing Nuclear Dynamics in Momentum Space: A New Interpretation of (e, 2e) Electron Impact Ionization Experiments on Ethanol

Balázs Hajgató,[†,‡] Michael S. Deleuze,*[,†] and Filippo Morini[†]

Research Group of Theoretical Chemistry, Department SBG, Hasselt University, Agoralaan Gebouw D, B-3590 Diepenbeek, Belgium, and Eenheid Algemene Chemie, Vrije Universiteit Brussel, Faculteit Wetenschappen, Pleinlaan 2, B-1050 Brussels, Belgium

Received: March 25, 2009; Revised Manuscript Received: April 27, 2009

Calculations of electron momentum distributions for equilibrium geometries, employing advanced Dyson orbital theories and statistical thermodynamics beyond the RRHO approximation, fail to quantitatively reproduce the outermost momentum distribution profile inferred from (e, 2e) electron impact ionization experiments on ethanol employing high-resolution electron momentum spectroscopy. A very detailed study of the influence on this momentum distribution of nuclear dynamics in the initial ground state and in the final ionized state is presented according to a thermal averaging over exceedingly large sets of model structures as well as Born−Oppenheimer molecular dynamical simulations on the potential energy surface of the radical cation. Our results give very convincing albeit qualitative indications that the strong turn-up of the (e, 2e) ionization intensities characterizing the highest occupied molecular orbital (HOMO) of ethanol at low electron momenta is the combined result of (1) the extraordinarily flat nature of the conformational energy map of ethanol, which enables significant departures from energy minima in the ground electronic state, (2) strong anomeric interactions between an oxygen lone pair and the central C−C bond for the minor but significant fraction of conformers exhibiting a hydroxyl torsion angle (α) at around 90°, and, last but not least, (3) the possibility to observe with this minor conformer fraction ultrafast and highly significant extensions of the central C−C bond, resulting, in turn, in an enhanced delocalization of the HOMO from the oxygen lone pair region onto the methyl group, immediately after the sudden removal of an electron. This charge transfer appears to occur at the very first stages, that is, within an effective time scale on the order of ∼10 fs, of an ultrafast dissociation of the ethanol radical cation into a methyl radical and a protonated form of formaldehyde.

Introduction

Electron momentum spectroscopy[1] is a powerful "orbital imaging" technique, which focuses on (e, 2e) binary electron impact ionization experiments ($M + e^-[E_0] \rightarrow M^+ + 2e^-$) at high kinetic energies ($E_0 = 1.2$ keV, or more). With this technique, orbital momentum profiles can be experimentally inferred for atoms, molecules, and solids according to an angular analysis of electron counts in coincidence, in the form of one-electron transition momentum densities associated with specific ionization channels. This spectroscopy has been extensively employed during the past decade in order to study in momentum space the interplay of the molecular structure with orbital electron densities for conformationally versatile compounds such as *n*-glycine,[2,3] dimethoxymethane,[3,4] *n*-butane,[5,6] 1,3-butadiene,[7] 1-butene,[8] tetrahydrofurane,[9] ethylamine,[10] ethanethiol,[11] or ethanol.[12,13] It is now well-established that rotations of atoms or groups of atoms about single bonds may significantly influence the experimentally inferred momentum profiles, both in the inner- and outer-valence regions. This influence is often strong enough to justify the idea of using Electron Momentum Spectroscopy (EMS) for (qualitatively) probing the molecular conformation.[6] A most common (but risky) practice in this research field has consisted therefore in inferring the relative energy order and/or the relative abundances of conformers from a fitting of theoretical simulations employing standard Kohn−Sham orbitals onto experimental electron momentum profiles.[8−11]

However, as with any ionization spectroscopy, EMS experiments in vacuum are subject to many complications, and their interpretation requires extensive theoretical work if it has to have any value at all. Remembering the basic postulates of quantum mechanics, in particular, the probabilistic (Born) interpretation of (the square of) many-electron wave functions, and the (quantum mechanical) definition of most orbitals as eigenfunctions of effective (Hückel, Hartree−Fock, Kohn−Sham, etc.) one-electron Hamiltonian operators, one may rightly wonder whether the idea of "orbital imaging" is a provocation[14] or a modern adaptation ("imaging" or "imagining" orbitals?[14]) of the everlasting dilemma "to be or not to be". Do orbitals exist and can they be experimentally "reconstructed"?

In the context of EMS experiments, the idea of "orbital imaging" does bear relationships with some physical reality. The Born, electron binary encounter, weak coupling, and plane wave impulse approximations are most usually invoked for interpreting these experiments and justify, within an exact many-electron theoretical framework and a vertical depiction of ionization, a mapping of experimental (e, 2e) electron momentum distributions obtained at high electron impact energies, under noncoplanar symmetric kinematics, onto spherically averaged and resolution-folded Dyson orbital momentum distributions. In this framework, Dyson orbitals[15] are defined as partial overlaps between many-electron wave functions for the neutral ground state and the final ionized state. In most

* To whom correspondence should be addressed. E-mail: michael.deleuze@uhasselt.be.
† Hasselt University.
‡ Vrije Universiteit Brussel.

10.1021/jp9027029 CCC: $40.75
Published on Web 05/26/2009

applications of the theory onto one-electron ionization bands, experience with advanced many-body treatments and comparison with calculations employing density functional theory (DFT) show that, in practice, (normalized) Dyson orbitals can be rather accurately (but empirically) approximated by standard Kohn−Sham orbitals.[16,17] A first complication in the interpretation of EMS experiments often takes the form of a very strong dispersion of the ionization intensity over secondary shakeup lines that relate to electronically excited configurations of the cation and which may very substantially alter the electron momentum densities that are inferred from (e, 2e) ionization intensities at specific electron binding energies.[7,17] When the molecular target contains one or several rotatable bonds, another difficulty pertains to the usually rather strong influence of the molecular conformation onto electron binding energies.[7,18] Overlooking these difficulties may lead to astonishing contradictions[7] with elementary thermodynamics and other experimental determinations of the molecular structure. When the plane wave impulse approximation breaks down, the (e, 2e) ionization cross sections relate to mathematical transforms[19] involving distorted waves described as linear combinations of Coulomb waves,[20] in which case the experimentally inferred momentum distributions exhibit a significant dependence[21] on the kinetic energy of the impinging electron. At last, a recent EMS study of cyclopropane[22] seems to point out that Jahn−Teller distorsions, that is, ultrafast nuclear dynamics in the final state, may also lead to significant and recognizable fingerprints in the observed momentum distributions. Ultrafast nuclear dynamical processes, in the form of a cage fragmentation and a Coulomb explosion, have also been previously invoked in order to explain a tremendously strong rise of (e, 2e) ionization intensities at low momenta[23] in EMS experiments at the double ionization threshold of norbornane.[24] As shall be emphasized in the present contribution, significant deviations from a vertical picture of ionization can be safely identified from electron momentum distributions, provided the consequences of each approximation in the model are checked, either on experimental or theoretical grounds.

The molecular target in the present work is ethanol, probably the most useful organic molecule to mankind as a solvent, environmental friendly fuel,[25] and, last but not least, an essential component of wine. Experiments on this compound at various electron impact energies by means of an EMS spectrometer of the third generation[26] have been presented recently[12] and analyzed[13] according to the guidelines proposed in ref 4 or ref 18. In a first step, the (e, 2e) ionization spectra were thus unraveled on the grounds of quantitative calculations, within ∼0.2 eV accuracy, of valence one-electron and shakeup ionization energies and of the related Dyson orbitals[15] using the one-particle Green's function (1p-GF) theory[27] in conjunction with the so-called third-order algebraic diagrammatic construction scheme [ADC(3)],[28] as well as large basis sets incorporating diffuse functions. In the next step, thermally and spherically averaged momentum distributions at specific electron binding energies were computed from the corresponding Dyson orbitals, taking thereby into account the influence of the molecular conformation on electron binding energies and using conformer weights derived from other experiments or thermostatistical calculations[29] that account for the influence of hindered rotations.[30] These thermostatistical calculations were based on highly accurate estimates by Kahn and Bruce,[31] close to the full CI limit and incorporating corrections for scalar relativistic effects, of conformational energy differences. These led to estimates of 0.61 and 0.39 for the molar fractions characterizing the gauche (C_1) and anti (C_s) conformers at room temperature, respectively, in almost perfect match with the conclusions drawn[32] from a variety of spectroscopic (IR, microwave, core XPS) determinations of the molecular structure of ethanol, either in the gas phase or in highly diluted CCl_4 solutions. Using these molar fractions for computing resolution-folded, spherically, and thermally averaged Dyson orbital momentum distributions enabled us in turn[12,13] to accurately reproduce the momentum profiles characterizing most resolvable bands in the (e, 2e) ionization spectrum up to and beyond the shakeup onset at an electron binding energy of ∼24 eV.

Nevertheless, despite the high order attained in the treatment of electron correlation and relaxation, this first model based on the assumption of thermal equilibrium between two energy minima severely failed in quantitatively reproducing the experimental momentum distribution associated with the highest occupied molecular orbital (HOMO). The extremely limited dependence of the momentum distributions on the electron impact energy[12] rules out the possibility of a significant enough breakdown of the plane wave impulse approximation. In view of the very strong influence of the rotation of the hydroxyl group on the momentum distribution of the HOMO[12,13] and the extreme flatness of the conformational energy map of ethanol, it has been conjectured that this particularly pronounced discrepancy between theory and experiment could be the outcome of dynamical disorder,[12,13] that is, significant departures from the energy minima in the neutral ground state, due to temperature effects and internal molecular motions. According to MP4 calculations by Senent et al.,[33] ethanol is characterized indeed by exceedingly low hydroxyl torsion barriers, ranging from 404.1 (1.15 kcal/mol) to 423.3 cm^{-1} (1.21 kcal/mol), in practically perfect match with the results (1.15 kcal/mol) obtained for these barriers by a fitting of an asymmetric potential function onto observed torsional transitions in far-IR spectra.[34] The possibility of some experimental artifact is ruled out on the experimental side because almost identical results to those published by Ning et al. in ref 12 have been independently presented in a Ph.D. thesis at the University of Hefei, in Anhui, China, under the supervision of Prof. X. J. Chen.[35]

According to figures presented in this latter work and as was suggested in our previous contributions[12,13] already, an excellent match between theory and experiment is amenable for the HOMO of ethanol by considering relative abundances of 80 and 20% for the gauche (C_1) and anti (C_s) conformers, respectively. Before all, in order to emphasize the dangers that are inherent to such fitting procedures, we invite the reader to consider Figure 1, in which results of ref 13 are reemployed in order to simulate the electron momentum profiles characterizing the six outermost ionization bands in the (e, 2e) ionization spectra of ethanol[12] using various and arbitrary C_1/C_s conformer ratios. A C_1/C_s ratio of 80/20 is not only irrelevant from a thermodynamic viewpoint, it also fails in providing consistent insights for all ionization bands. Indeed, it is clear, upon examining Figure 1, that fitting theory onto the experimental results for the HOMO implies a deterioration of the quality of the theoretical predictions for most other bands. One noticeable exception pertains to the third band at 13.6 eV, for which the best agreement is obtained by using a C_1/C_s ratio of ∼4. This is most certainly the consequence of rather strong overlaps with bands (2) and (4) at 12.4 and 15.8 eV and of the very strong conformational dependence of the ionization energy characterizing two orbitals in this range of electron binding energies (see Figure 2 in ref 13), which makes the analysis of ionization intensities in this energy region particularly cumbersome.

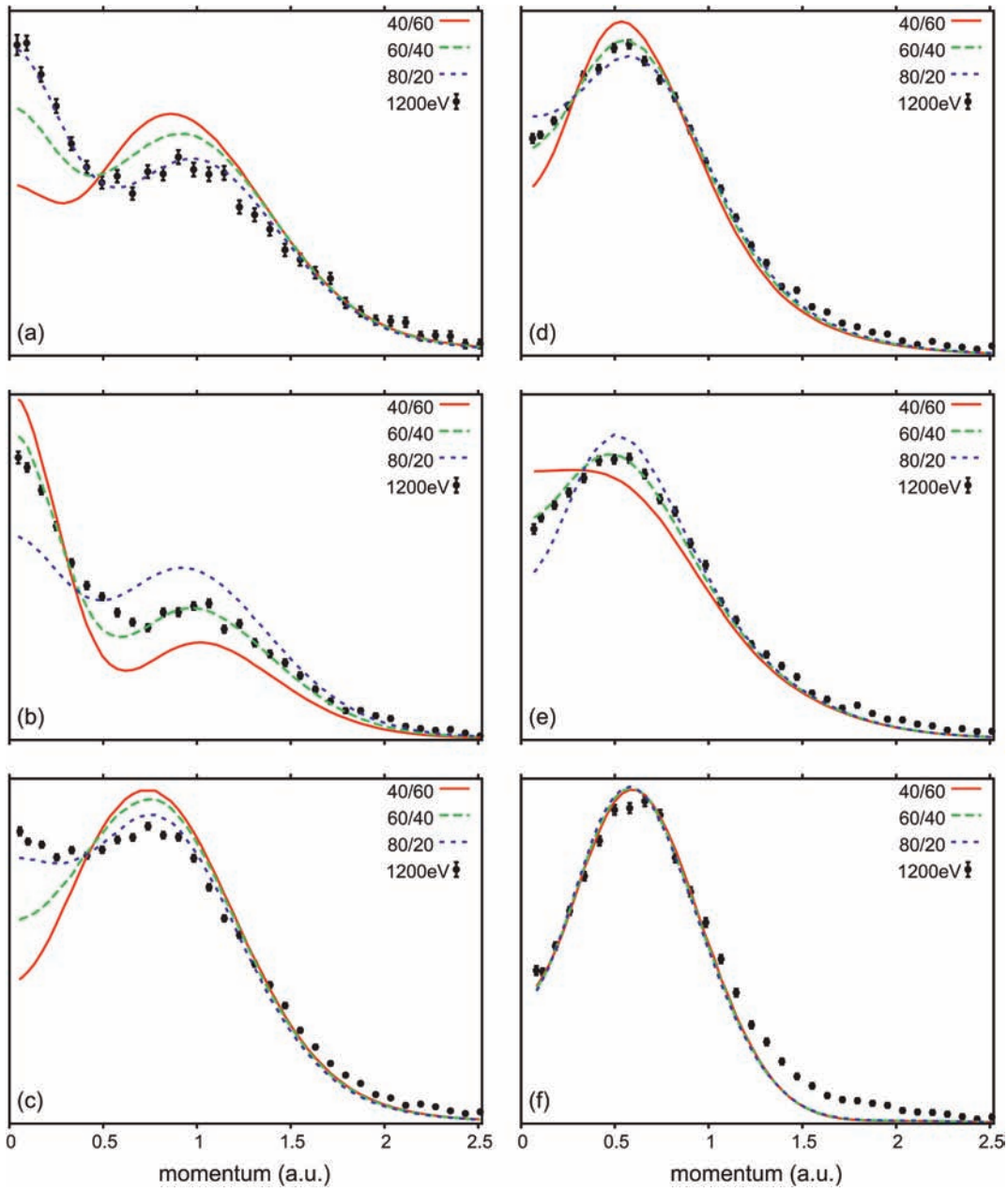

Figure 1. Evolution of the Dyson orbital momentum distributions characterizing, at the ADC(3)/cc-pVDZ++ level,[12] the six outermost ionization bands in the (e, 2e) measurements by Ning et al. at $E_0 = 1.2$ keV upon various C_1 to C_s ratios of conformer abundances and comparison with the experimentally inferred profiles.[12]

Clearly, improved structural and dynamical models are required for enabling consistent insights into the experimental electron momentum distributions, and this is throughout the valence ionization spectrum of ethanol.

Our present purpose is therefore to examine in detail the influence of nuclear dynamics, both in the initial ground state and in the final ionized state, on the outermost electron momentum distribution characterizing ethanol in (e, 2e) electron impact ionization experiments. In a first step, thermal averaging of the momentum profile for this level is extended to large sets of model molecular structures containing up to 1728 entries, in order to account for all possible transitions between the two energy minima of the molecule of interest through the interplay of combined hydroxyl and methyl rotations. In the next step, the influence of geometrical relaxation effects is qualitatively investigated in the final state on the grounds of calculations employing Born−Oppenheimer molecular dynamics.[36] The final picture that emerges from these calculations is that both aspects of nuclear dynamics need to be considered for reconciling theory with experiment.

Computation Section

In this work, we simulate the outcome of EMS experiments performed upon ethanol using a standard (e, 2e) noncoplanar symmetric kinematical setup at an electron impact energy of 1.20 keV above the vertical ionization energy threshold (VIE $\sim$ 10.88 eV). For the sake of conciseness, we must refer the interested reader to textbooks and previous works[1,4−7,13] for detailed presentations of the underlying theory. According to the characteristics of the employed (e, 2e) spectrometer,[12] the relevant parameters for the momenta of the impinging and outgoing electrons amount to $p_0 = 0.271105(1200 + \mathrm{VIE})^{1/2}$ au (1 au = 1 a_0^{-1}, with a_0 as the Bohr radius, i.e., 0.5292 Å)

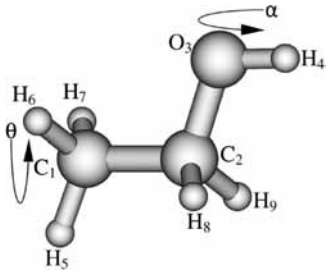

Figure 2. Structural characterization and main torsional characteristics of the molecular target.

and $p_1 = p_2 = 6.64077$ au, respectively ($E_1 = E_2 = 600$ eV). In view of the employed kinematics, which favors clean knocked-down collision processes, and because of the very limited dependence of the (e, 2e) ionization cross sections onto the impinging kinetic energy, as well as the large spectroscopic strength for the outermost ionization process, we can safely invoke the binary (e, 2e) encounter, plane wave impulse, and target Kohn−Sham approximations,[1] in conjunction with calculations employing DFT[37] and the standard Becke three-parameter Lee−Yang−Parr (B3LYP) functional.[38] The target Kohn−Sham approximation is perfectly justified in this case because of the almost perfect match between the (normalized) Dyson ADC(3) and Kohn−Sham (B3LYP) momentum distributions characterizing the highest occupied molecular orbitals of the two conformers.[12,13] In the present work, we will thereby evaluate the dependence upon the azimuthal angle, that is, the electron momentum dependence, of the (e, 2e) ionization cross sections for the lowest ionized state of ethanol, according to spherically averaged and resolution-folded structure factors obtained from the square of the Fourier transforms of standard B3LYP Kohn−Sham orbitals.

Most results presented in this work have been obtained according to single-point DFT calculations using the B3LYP functional, in conjunction with Dunning's augmented correlation-consistent polarized valence basis set of triple-ζ quality[39] (i.e., the B3LYP/aug-cc-pVTZ level). These calculations have been performed upon (//) geometries that were optimized at the B3LYP/aug-cc-pVDZ level, under the constraint of fixed torsional parameters (Figure 2), in order to enforce controlled rotations of the hydroxyl and methyl groups. From here and henceforth, these rotations will be defined according to the following dihedral angles: $\alpha = 180° - \tau(C_1-C_2-O_3-H_4)$ and $\theta = 180° - \tau(H_5-C_1-C_2-O_3)$. According to this definition, note that the global energy minimum (C_s, trans) form of ethanol is characterized by $\alpha = \theta = 0.0°$, whereas the gauche conformer, of C_1 symmetry, is characterized by $\alpha = 118.3°$ and $\theta = 2.4°$ (B3LYP/aug-cc-pVTZ results).

In the sequel, comparison will be made between three different structural models of the molecule in its neutral electronic ground state. The first model is the static one used in refs 12 and 13, which is based on the assumption that thermodynamical equilibrium prevails between the two energy minima, assuming thereby C_1 and C_s molar fractions of 0.607 and 0.393, respectively [all results obtained by means of this model pertain to fully optimized B3LYP/aug-cc-pVTZ geometries (Table 1 and Figure 2)]. In the second or third models, referred further to as the one- or two-dimensional (1D or 2D) models, we consider thermal averaging over a set of 72 model structures characterized by α angles ranging from −180 to 175° in steps of 5° or over a set of 1728 model structures characterized by α angles ranging from −180 to 175° and by θ angles ranging from −55 to +60°, again in steps of 5°. The torsional

TABLE 1: Structural Parameters of Ethanol in Its Neutral Ground State and after Ionization[a]

	point group				
	experiment[b]		neutral		cation
structural parameters	C_1	C_s	C_1	C_s	C_1
C_1-C_2	1.512(3)	1.499(3)	1.52	1.51	1.76
C_2-O_3	1.422(2)	1.431(2)	1.43	1.43	1.33
O_3-H_4	0.85(3)	0.79(4)	0.96	0.96	0.98
C_1-H_5	0.96(4)	0.93(3)	1.09	1.09	1.09
C_1-H_6	1.05(4)	1.01(3)	1.09	1.09	1.08
C_1-H_7	1.01(3)	0.95(3)	1.09	1.09	1.08
C_2-H_8	1.04(3)	0.96(3)	1.07	1.10	1.09
C_2-H_9	0.93(3)	0.98(3)	1.09	1.10	1.09
$C_1-C_2-O_3$	112	108.8	113.0	108.1	106.3
$C_2-O_3-H_4$	102	107	108.9	109.1	114.1
$H_5-C_1-C_2$	115	113	110.6	110.4	99.5
$H_6-C_1-C_2$	113	114	111.1	110.6	104.9
$H_7-C_1-C_2$	109	109	110.7	110.6	105.1
$H_8-C_2-C_1$	107	115	110.4	110.2	103
$H_9-C_2-C_1$	118	117	110.4	110.2	99.3
$H_8-C_2-O_3$	110	112	110.3	110.3	116.4
$H_9-C_2-O_3$	104	109	105.0	110.3	110.6
$C_1-C_2-O_3-H_4$	63 ± 2	179 ± 2	61.7	180.0	94.4
$H_5-C_1-C_2-O_3$			177.6	180.0	176.1
$H_6-C_1-C_2-O_3$			−63.0	−59.95	−64.8
$H_7-C_1-C_2-O_3$			+57.3	+59.95	+56.8
α			118.3	0.0	85.6
θ			2.4	0.0	3.9

[a] Bond lengths are in Å, and bond and torsion angles are in degrees (B3LYP/aug-cc-pVTZ results). [b] Uncorrected X-ray diffraction data, taken from Jönsson, P.-G. Acta Crystallogr., Sect. B 1976, 32, 232.

modes are considered to be independent structural parameters and to define therefore fixed (or "clamped") independent nuclei configurations within the framework of the Born−Oppenheimer approximation. This assumption about the independence of the α and θ parameters allows us to compute conformer weights at room temperature ($T = 298.15$ K) according to Boltzmann statistical thermodynamics ($k_B = 1.38054\ 10^{-23}$ J K^{-1}), that is

$$w_i(\alpha) = \frac{e^{-E(\alpha_i)/k_BT}}{\sum_{i=1}^{72} e^{-E(\alpha_i)/k_BT}} \quad (1)$$

or

$$w_i(\alpha, \theta) = \frac{e^{-E(\alpha_i,\theta_i)/k_BT}}{\sum_{i=1}^{1728} e^{-E(\alpha_i,\theta_i)/k_BT}} \quad (2)$$

where the sum over i runs over the above-defined sets of configurations. The employed force fields derive from the parametrization by Senent et al. against highly accurate single-point calculations of the corresponding 1D (hydroxyl) or 2D (hydroxyl and methyl) torsional energy curves (see eqs 11 and 14 in ref 33) at the level of fourth-order Møller−Plesset perturbation theory incorporating double, triple, and quadruple substitutions [MP4(SDTQ,Full)], upon MP2 geometries, in conjunction with Dunning's correlation-consistent basis set of triple-ζ quality (cc-pVTZ).

Summarizing our methodology so far, spherically averaged Dyson orbital momentum distributions have been computed for the highest occupied molecular orbital using the above conformer weights for thermally averaging the individual conformer

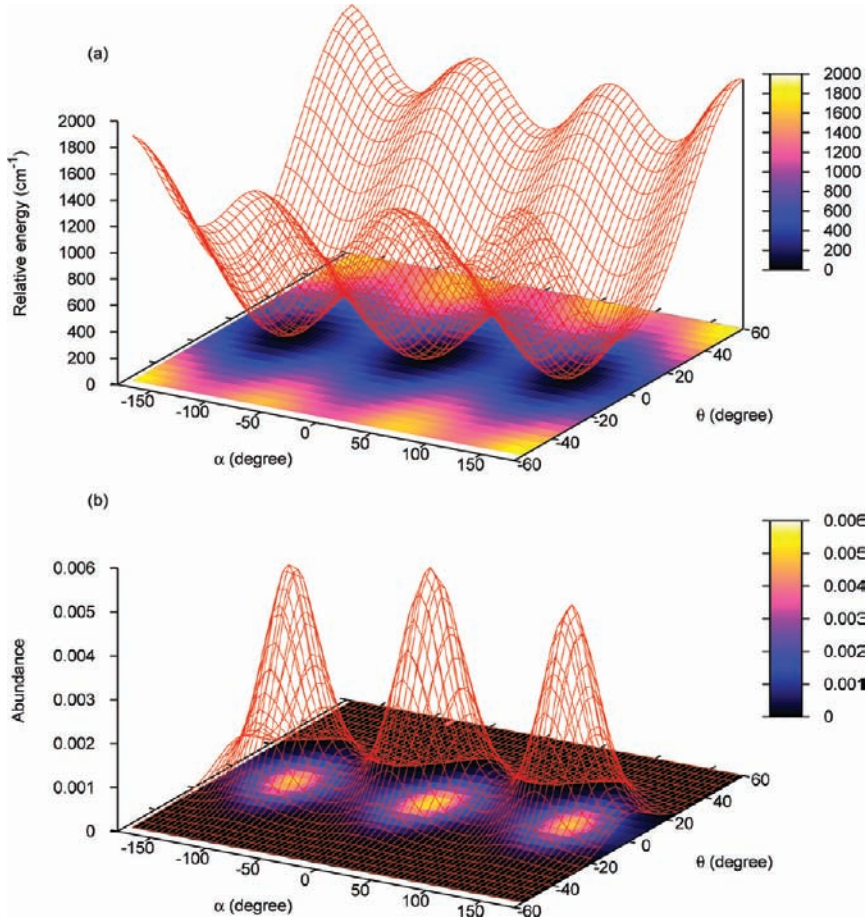

Figure 3. Conformational energy map and related conformer distributions, according to the force field by Senent et al.[33]

contributions. The latter were specifically obtained according to the target KS approximation and single-point calculations of the electronic wave function at the B3LYP/aug-cc-pVTZ level, upon B3LYP/aug-cc-pVDZ fully optimized geometries, under the constraint of fixed torsional (α, θ) parameters. We note here that our analysis of the influence of molecular dynamics in the ground state is greatly facilitated by the fact that with all selected "clamped" nuclear configurations, the HOMO remains well-isolated and lies at ~1.6 eV above the next orbital. Also, its energy remains almost independent of the molecular conformation. In view of an experimental energy resolution of ~0.6 eV,[12] there is thus in this case clearly no risk of spectral contamination by shakeup lines and overlap with higher-lying ionization bands.

The last step that is required for a consistent analysis of the influence of ground-state nuclear dynamics on the experimentally inferred momentum densities implies resolution folding of the finally obtained thermally and spherically averaged momentum distribution. This has been achieved by means of a procedure employing Monte Carlo simulations[40] in order to account for the limited experimental resolution in momentum space. In line with the characteristics of the previously employed experimental set up, we retained a tolerance of ± 0.84 and ± 0.57° on the azimuthal and polar angles, respectively, which implies a momentum resolution of $\Delta p \sim 0.16$ au (fwhm) or ~0.069 au (one standard deviation) at an impact energy of 1.2 keV. We independently checked on the 1D model that thermal averaging of resolution-folded, spherically averaged momentum profiles gave virtually identical results, as it should.

A preliminary and mainly qualitative study of nuclear dynamical (i.e., molecular relaxation) effects in the final state and of their influence on the outermost electron momentum distribution is thereafter presented on the same theoretical and methodological grounds according to (1) optimizations of the geometry of the radical cation at the B3LYP/aug-cc-pVTZ level (Table 1), (2) a scan, at the B3LYP/aug-cc-pVDZ level, of the potential energy surface of ethanol$^+$ over the above 2D series of (α,θ) torsion angles, and, at last, (3) Born−Oppenheimer molecular dynamical (BOMD) calculations,[36] at the same B3LYP/aug-cc-pVDZ level, of the evolution in time of the system immediately after ionization. The trajectory step size was set to 0.250 au, the Bulirsch−Stoer method was used for the integration scheme,[41] along with an integration step size of 0.2 fs, and a fifth-order polynomial fit in the integration correction scheme was used. All BOMD trajectory calculations have been performed at 0 K. We thereby neglect thermal motions in the final ionized state, that is, we assume that the only source of kinetic energy immediately after ionization exclusively arises from potential energy gradients. This approximation is perfectly justified when comparing the extent of thermal fluctuations at room temperature ($k_BT \sim 25$ meV) with ionization energies larger than 10 eV and an energy resolution on the order of 0.6 eV.[12]

The alterations that the electronic wave function undergo during these nuclear relaxation processes have been correspondingly quantified at the same level, according to calculations of atomic charges and Wiberg bond orders,[42] within the framework of a natural bond orbital (NBO) analysis.[43] Total bond orders have been calculated by summing the values derived from the α- and β-spin electron densities in the matrix of Wiberg indices.[44]

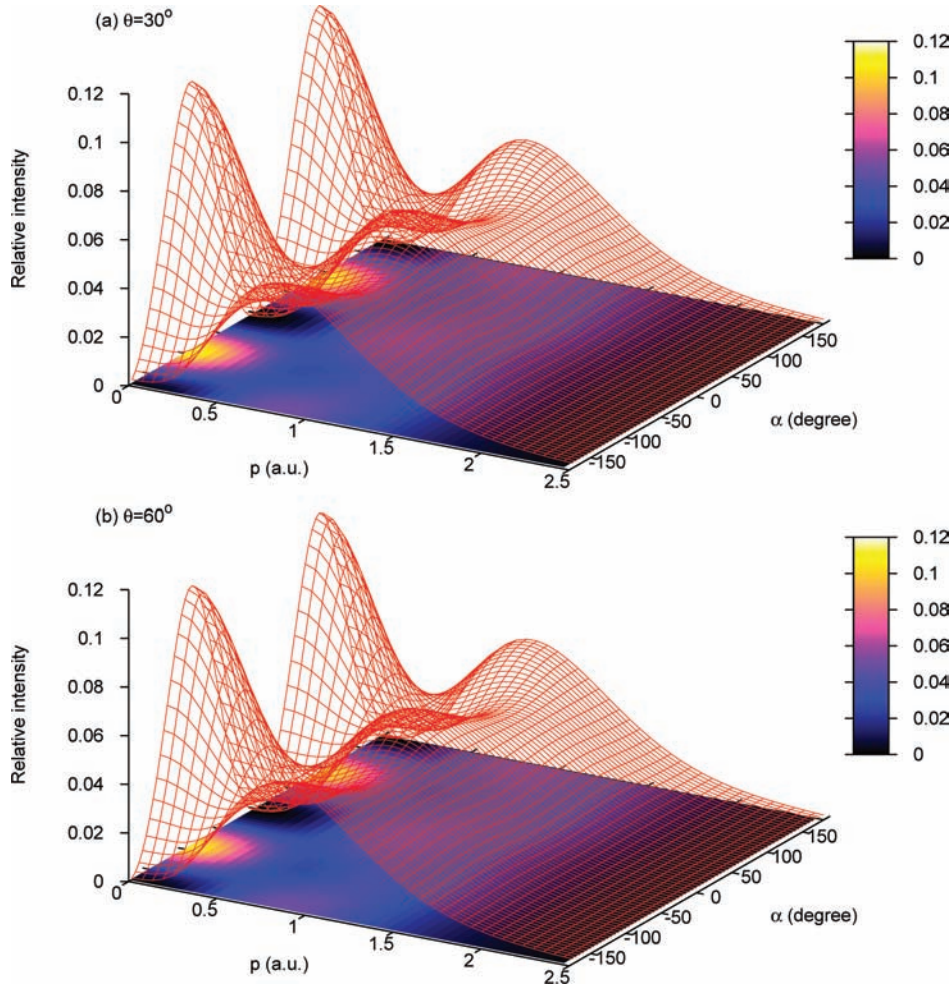

Figure 4. Evolution of the outermost momentum profile of ethanol as a function of the hydroxyl (α) torsion angle (B3LYP/aug-cc-pVTZ//B3LYP/aug-cc-pVDZ results).

Results and Discussion

Orbital Imaging of Molecular Dynamics in the Neutral Ground State. A plot of the conformational energy map of ethanol is presented in Figure 3, according to the parametrization by Senent et al.,[33] along with the conformer abundances that were correspondingly computed according to eq 2. Note that by virtue of the selected range of α-angles, the double multiplicity of the energy minimum accounting for the gauche (C_1) conformer is explicitly accounted for. It is immediately apparent that the extreme flatness of this potential energy surface and the very low energy barriers for the trans−gauche and gauche−gauche conversions, which amount to 404.1 (1.15 kcal/mol) and 423.3 cm^{-1} (1.21 kcal/mol), result in an extremely strong broadening of the conformer distributions around energy minima. Close to these minima, the broadening appears to be "isotropic", that is, on the same order of magnitude, with respect to the hydroxyl and methyl rotations. Note, in particular, that the relative abundances of conformers in the transition regions are small but not insignificant at room temperature. For instance, regardless of symmetry and multiplicity factors, the weight of the ($\alpha = 60°$, $\theta = 0°$) nuclear configuration at 298 K amounts to 14%, relative to the abundance of the trans (C_s) global energy minimum. This observation certainly motivates detailed and systematic investigations of the influence of the rotation of the hydroxyl and methyl groups on the momentum distributions characterizing the HOMO for each conformer in the selected ensembles.

In Figure 4, we disclose in a three-dimensional plot the spherically averaged electron momentum profile of the HOMO as a function of the α (hydroxyl) torsion angle at two different values (30 and 60°) for the θ (methyl) torsion angle. This figure confirms the extremely strong influence of hydroxyl rotation on the outermost electron momentum profile,[12,13] in particular, at low momenta. In both cases, the maximal turn-up in the electron momentum density characterizing the HOMO at $p \rightarrow 0$ is observed when $\alpha = \pm 90.0°$.[12] It is thus here certainly worth noticing that, relative to the global energy minimum (C_s) form, the weight of the ($\alpha = 90°$, $\theta = 0°$) nuclear configuration amounts to ∼33%, regardless of the double multiplicity of this nuclear configuration. In contrast, and in line with the A″ and thus p-type symmetry of the HOMO of ethanol in the trans (C_s) form, the corresponding momentum orbital density at $p \rightarrow 0$ au almost identically vanishes when $\alpha = 0°$,[12,13] despite the release of symmetry constraints due to departures from $\theta = 0°$, that is, methyl rotations.

The latter observation already sheds some light on the results displayed in Figure 5, in which spherically averaged orbital densities are plotted at two specific values of the electron momentum parameter as a function of the α (hydroxyl) and θ (methyl) torsion angles. This figure confirms in both cases that the momentum profile characterizing the HOMO is extremely sensitive to rotations of the hydroxyl group, whereas rotations of the methyl group appear to have only marginal consequences.

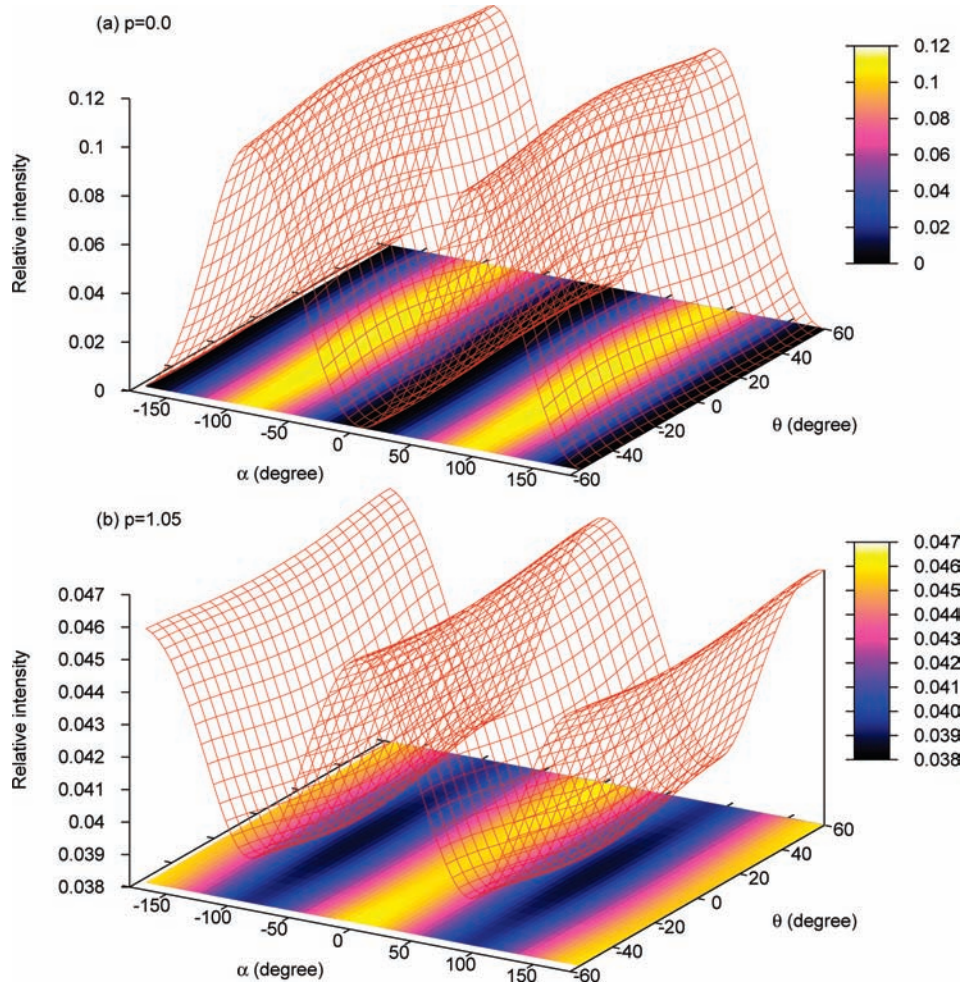

Figure 5. Evolution of the spherically averaged outermost momentum density of ethanol at specific values of the target electron momentum (p) as a function of the hydroxyl (α) and methyl (θ) torsion angles (B3LYP/aug-cc-pVTZ//B3LYP/aug-cc-pVDZ results).

The rationale for these observations is to be found in the contour plots that are presented for various nuclear configurations in Figure 6. In line with these observations, it is clear that rotations of the methyl group have almost no influence on the topology and spread of the highest occupied molecular orbital, which pertains essentially to a rather strongly localized oxygen lone pair. When α lies at around 0 or 180°, some delocalization is observed on the vicinal C−H bonds as a result of anomeric interactions between the oxygen lone pair and the emptied σ^* (C−H) orbital, according to a localized (e.g., NBO) depiction of chemical bonds. In contrast, when α lies at around 90°, delocalization extends onto the central C−C bond, this time because of anomeric interactions with the associated σ^* orbital. These changes in the delocalization pattern of the HOMO when α evolves from 0 to 90° and the conversion thereby of two perpendicular nodal surfaces (d_{xy} topology, i.e., A″ symmetry under the C_s point group) into two or three apparent parallel nodal surfaces ($\sim d_z^2$ or $\sim f_z^3$ topology, with an effective mirror symmetry with respect to the $C_1-C_2-O_3$ plane) are most clearly at the origin of the reversal of the outermost electron momentum distribution from a p-type to a mixed s−p-type profile, characterized by one minimum, at $p \sim 0.0$ and 0.6 au, and by one and two maxima, at $p \sim 0.6$ au and 0.0 and ∼1.1 au, respectively. MO topologies and anomeric interactions provide therefore a straightforward explanation of the maximal turn-up of the outermost electron momentum densities at $p \rightarrow 0$ when α ∼ 90°.

In view of the results displayed in Figures 3 and 4, it is most natural to expect a strong influence of molecular dynamics in the electronic ground state on the momentum densities that were experimentally reconstructed from an angular analysis of the (e, 2e) ionization cross sections. The final results of our study so far are presented in Figure 7, in the form of resolution-folded, spherically, and thermally averaged momentum distributions, according to the three structural models of ethanol presented in the preceding section. Clearly, the three models provide essentially similar results because of an accidental (and, thus, a priori unpredictable) cancellation of all of the changes in the momentum profile which occur with the rotation of the hydroxyl group as α evolves from 0 to 180° (Figure 4; see also Figure 4 in ref 12). Note furthermore that the 1D and 2D thermal averages provide strictly identical results, an observation which is in line with the oxygen lone pair nature of the HOMO. Whatever the employed model for describing the structure of ethanol in the gas phase, the agreement between all theoretical results and the experimental results by Ning et al.[12] remains highly deceptive. Lacking other reliable explanations, ultrafast nuclear dynamics in the final ionized state must be invoked for explaining this most puzzling discrepancy with experiment. As shall be seen in the next section, thermal motions in the neutral ground state appear nonetheless to be a key ingredient for unraveling nuclear dynamics after ionization, and the reader may already be reassured that the results of the present section will find their place in the final interpretation.

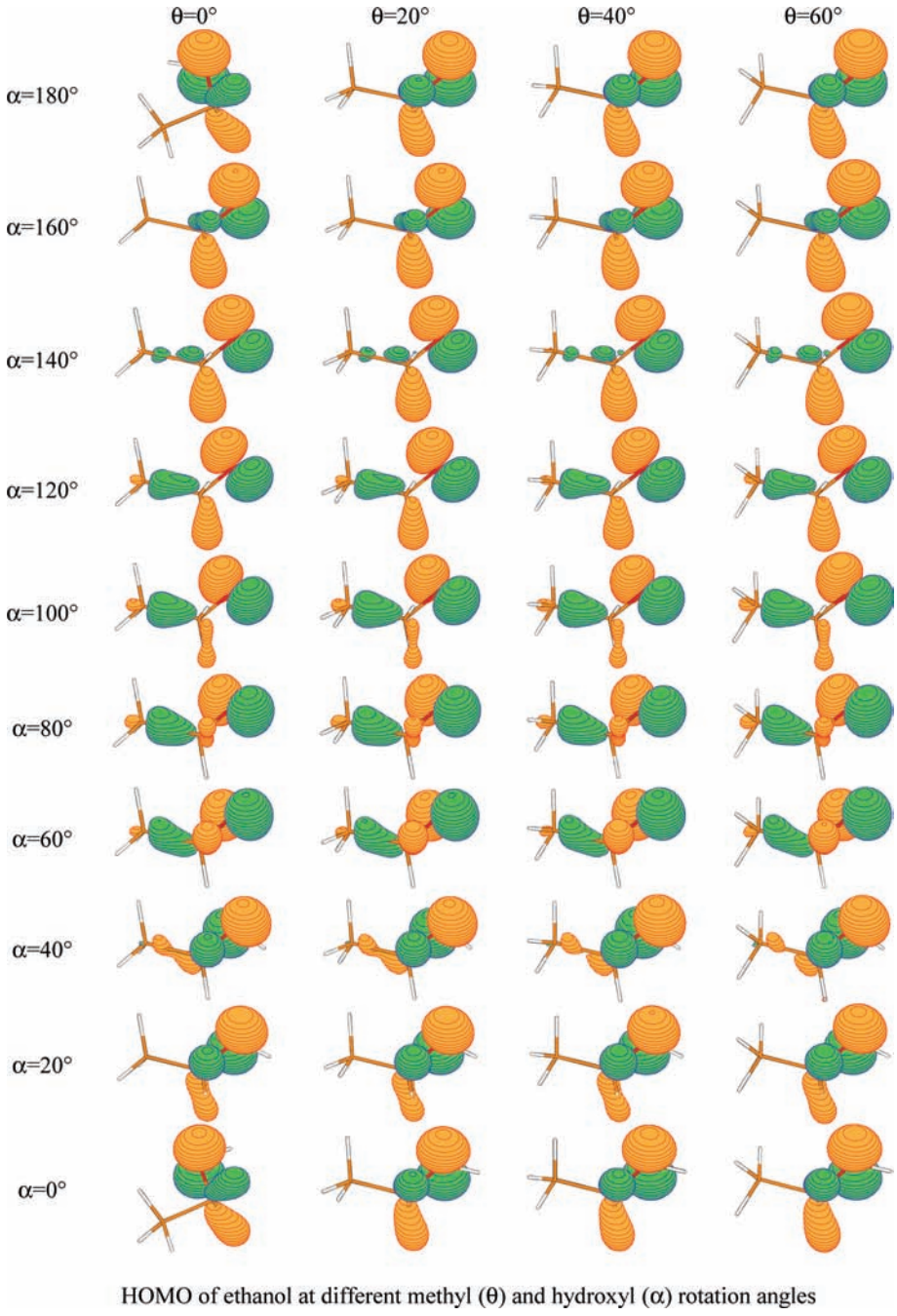

Figure 6. Evolution of the highest occupied molecular orbital (HOMO) of ethanol as a function of the hydroxyl (α) and methyl (θ) torsion angles (B3LYP/aug-cc-pVTZ//B3LYP/aug-cc-pVDZ results).

Compared with deeper-lying orbitals, ionization of the highest occupied molecular orbital of ethanol is expected, in view of its stronger localization as an oxygen lone pair, to result into stronger, and thus faster, relaxation processes. This is certainly true from an electronic viewpoint, as a comparison of Koopmans's and OVGF (outer valence Green's function) estimates of electron binding energies demonstrates (Figure 8). Whereas electronic correlation and relaxation corrections amount to a lowering by ~1 eV for the HOMO (13a, alias 3a″ orbital for the C_s form), the shift downward does not exceed 0.7 eV for the HOMO-1 (12a, alias 10a′) and HOMO-2 (11a, alias 2a″) levels.

Prior to considering the consequences of geometrical relaxations in the final state, one may wonder whether this discrepancy between theory and experiment could not be explained by highly fancy scenarios involving tunneling effects or the formation of molecular clusters. It is, in our opinion, extremely unlikely that such scenarios will quantitatively improve our understanding of EMS experiments on ethanol. Indeed, according to results by Shundalov et al.,[45] tunneling wavepacket dynamics in π-periodic potentials, which are very much comparable to that describing the hydroxyl rotation in ethanol, occurs within a time scale on the order of 333 ps, to compare with thermal conversion rates on the order of 5.6 transitions per picoseconds at 298 K, according to an application of elementary transition-state theory onto barriers on the order of 1.15 kcal/mol. Tunneling occurs thus at a much too slow pace to have really some significance. Also, the corresponding energy splitting is extremely minute, on the order of a few cm^{-1}, and can usually only be detected with microwave spectroscopy.[46]

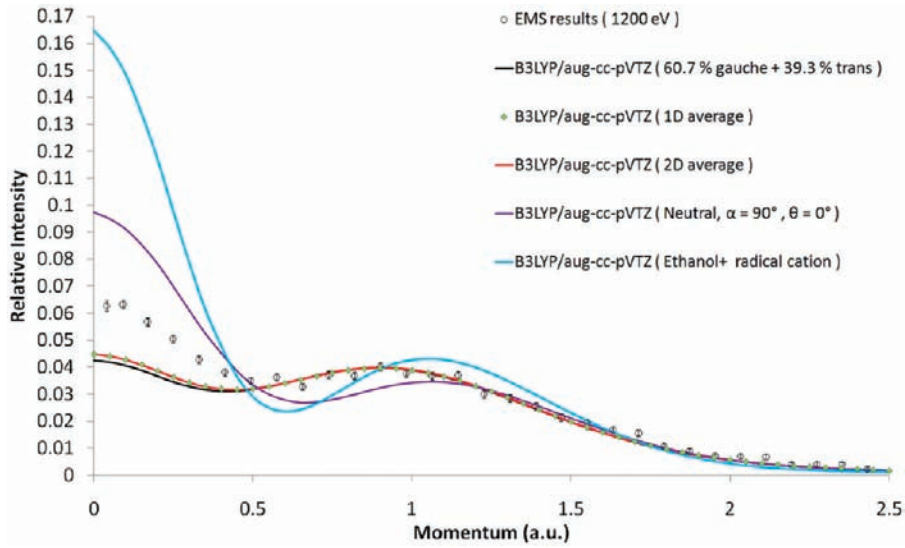

Figure 7. Comparison against the experimental profile at $E_0 = 1.2$ keV[12] of resolution-folded and spherically averaged momentum density distributions for the HOMO, obtained using three different models for thermal averaging (see Computation Section) or the results of restricted (closed-shell) B3LYP/aug-cc-pVTZ calculations upon the geometry characterizing the ($\alpha = 90°$, $\theta = 0°$) configuration on the potential energy surface of the neutral or upon the relaxed geometry of the radical cation. Note in the latter case that the particularly strong enhancement of the momentum densities at $p \rightarrow 0$ and 1.1 au reflects a very significant stretching of the C_1-C_2 bond.

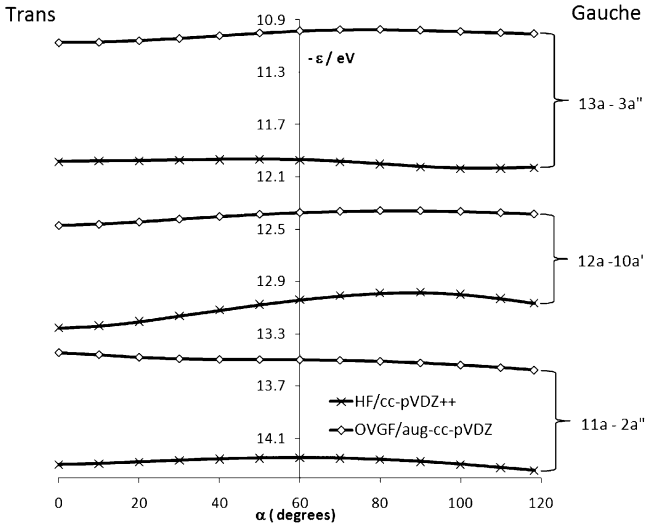

Figure 8. Comparison of HF (Koopmans's theorem) and OVGF estimates for the electron binding energies characterizing the three outermost orbitals of ethanol, as a function of the hydroxyl (α) rotation angle.

The formation of dimers of ethanol molecules is energetically favored in view of a binding energy of ~5.0 kcal/mol (MP2/6-311++G(3df,2p) result, including counterpoise and vibrational zero-point corrections[47]) but remains most improbable under high-vacuum conditions because of highly unfavorable entropy effects. Very specific conditions, as for instance in supersonic molecular beams,[48] need to be met for experimentally studying such clusters. Besides, the formation of dimer complexes should tremendously affect the ionization spectrum and the related (canonical) electron momentum distributions, not only for the HOMO but throughout the valence region. This is obviously at odds with experimental evidence (see, e.g., Figure 1).

Orbital Imaging of Molecular Dynamics in the Final Ionized State. Oxygen-containing radical cations are known, for a long time already, to exhibit unusual C−C bonds as long as 2.0 Å,[49] and, whatever the employed theoretical model, ethanol makes no exception to the rule (ref 50; see also Table 1). For this compound, whatever the starting geometry, an adiabatic ionization process does not only result in a highly significant lengthening of the C−C bond but also in considerable changes of the torsion characteristics in the form of a rotation of the hydroxyl group to $\alpha = 86°$. These structural alterations induce, in turn, extremely significant alterations of the underlying electron densities, in the form of an overwhelmingly strong turn-up of the (normalized) outermost electron momentum density at $p \rightarrow 0.0$ and $p \sim 1.1$ au (Figure 7). It is, in particular, very clearly apparent from the latter figure that such a lengthening of the C−C bond will strongly enhance the changes that occur in the momentum density upon rotation of the O−H group at $\alpha \sim 90°$. The final outcome of an adiabatic (i.e., on an infinitely long time scale) transition at 0 K would be an increase by a factor of ~4 (!) of the spherically averaged and resolution-folded orbital density at $p \rightarrow 0$, compared with a vertical depiction of ionization upon thermally averaged sets of molecular structures at 298.15 K. In view of this most impressive result and despite the very limited time scales under which (e, 2e) electron impact ionization events at high kinetic energies are expected to take place, it is more than reasonable to admit that even incomplete (i.e., on short time scales) geometrical relaxation effects could account for the discrepancies that are observed between theory and experiment for the electron momentum density characterizing the HOMO. Precise estimates of these time scales remain highly elusive for the moment. At this stage, it suffices to note that evidence starts to accumulate in the EMS literature[22−24,51] regarding significant deviations from vertical depictions of ionization in (e, 2e) processes, possibly as a result of a lack of resolution in time in measurements of electron counts that need to be performed in coincidence.

Prior to investigating nuclear dynamics in the final state, it is useful to compare (Figure 9) the conformational energy maps of ethanol in its neutral ground state and its vertical as well as adiabatic ionized states. The energy map displayed in Figure 9a is the result of B3LYP/aug-cc-pVDZ geometry optimizations for the neutral under the constraint of fixed torsional (α, θ) characteristics. Note that this map is essentially the same as that inferred by Senent et al.[33] at the MP4/cc-pVTZ//MP2/cc-pVTZ level, except for a reduction of the global energy scale

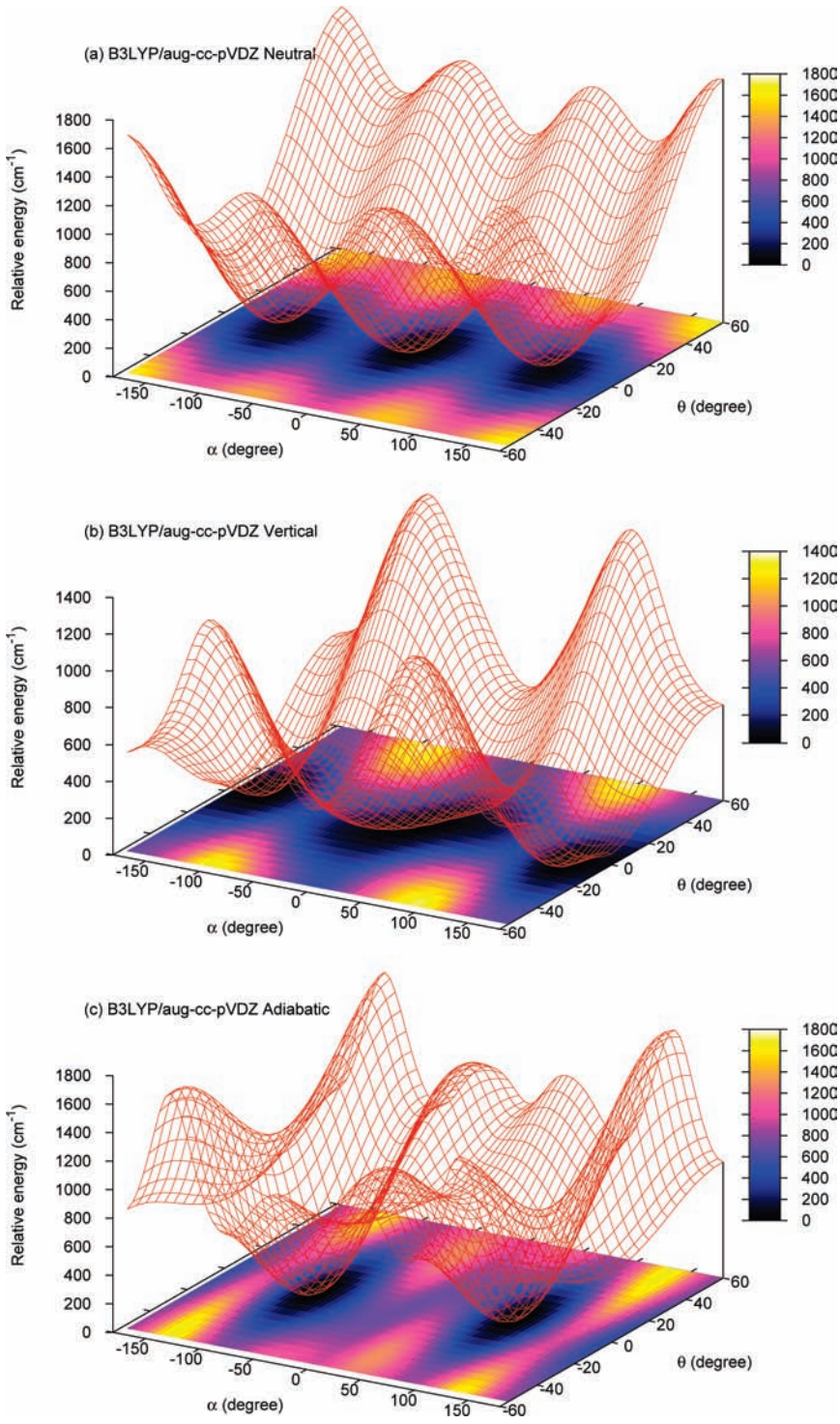

Figure 9. Comparison of the conformational energy map of ethanol (a) in its neutral ground state, (b) in its vertical ionized state, (c) and in its adiabatic ionized state (B3LYP/aug-cc-pVDZ results).

by ~10%. The energy map displayed in Figure 9b is the result of single-point B3LYP/aug-cc-pVDZ calculations for the radical cation on the geometries that were optimized for the neutral, again under the constraint of fixed torsional (α,θ) characteristics. Except for a reduction of the energy scale and a substantial flattening around minima, this map is qualitatively the same as the one for the neutral. Since forces and accelerations are determined by energy gradients, it is then rather clear that the torsional characteristics of the trans and gauche energy minima in the conformational energy map of the neutral are not going to be straightforwardly affected by the (instantaneous) removal of an electron in the HOMO. In line with this remark, examination of Figure 9c is particularly instructive. In this figure, we present the results of geometry optimizations for the radical cation, again at the B3LYP/aug-cc-pVDZ level and once more under the constraint of fixed torsional (α,θ) characteristics. It is clear that, after ionization and a readjustment of all bond lengths and angles, the gauche conformers ($\alpha = \pm\sim120°$) are found to lie near high-lying transition states, whereas the trans conformer ($\alpha = 0°$) strictly coincides with a low-lying transition state. There is also obviously only one nonredundant energy minimum ($|\alpha| = 86°$) on the conformational energy map of the

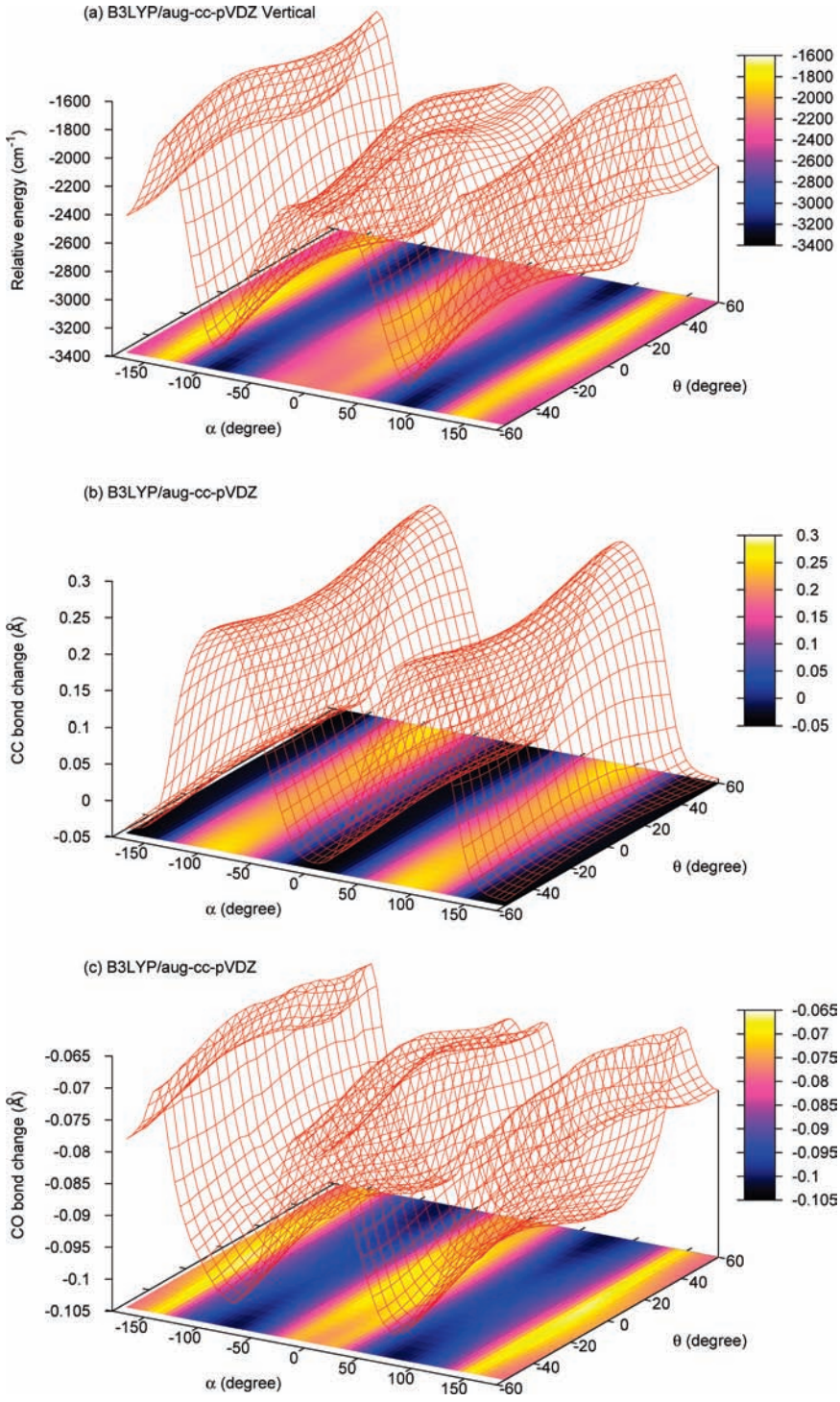

Figure 10. Evolution of the (a) relaxation energy and (b, c) changes in the C_1-C_2 and C_2-O_3 bond lengths as a function of the α (hydroxyl) and θ (methyl) torsion angles (B3LYP/aug-cc-pVTZ//B3LYP/cc-pVDZ results).

radical cation. From Figure 9b and c, it is thus already possible to guess that rotations of the hydroxyl group toward the $\alpha = \pm 86°$ position are a necessary prerequisite for a significant lengthening of the C−C bond and further enhancements thereby of the outermost electron momentum density at $p \rightarrow 0$ au!

To investigate this point in more detail, we consider in Figure 10 the changes that occur relative to the neutral and at the B3LYP/aug-cc-pVDZ level in the energy as well as in the C−C and C−O bond lengths upon optimization of the geometry of the radical cation, again under the constraint of fixed α and θ angles. Quite clearly, the molecular relaxation processes will not be affected very much by rotations of the methyl group. It is also most obvious that maintaining α torsion angles at around 0° will prevent strong relaxation effects, that is, fast nuclear dynamics. The strongest (or fastest) molecular relaxation processes will clearly be associated with torsions of the hydroxyl group to $\alpha = \pm 86°$, a position at which these processes take the form of a lengthening of the C−C bond by ∼0.25 Å, and, correspondingly, a shortening of the C−O bond by 0.1 Å. In view of the results displayed in Figures 9 and 10, it is thus most useful to remember that thermal motions in the ground state significantly populate the nuclear configurations characterized by hydroxyl torsion angles at around $\alpha = \pm 90°$.

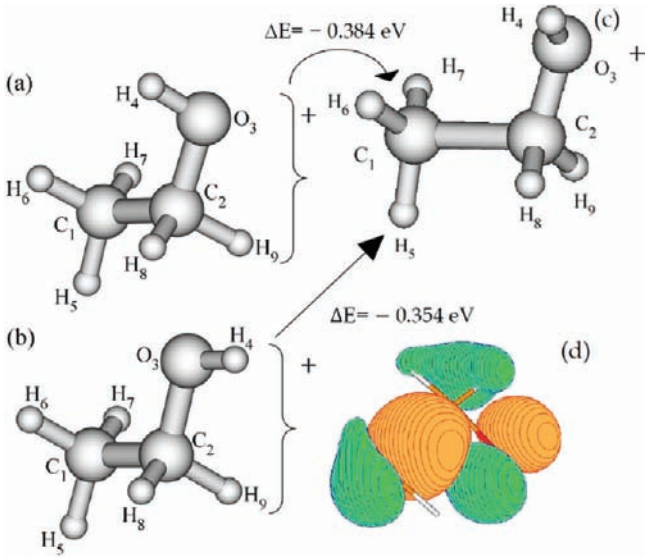

Figure 11. Structural, energetic, and electronic consequences of an adiabatic ionization process in ethanol; (a) C_1 (gauche) conformer, (b) C_s (trans) conformer, (c) radical cation, and (d) singly occupied molecular orbital of the radical cation (B3LYP/aug-cc-pVTZ results).

At the B3LYP/aug-cc-pVTZ level, the molecular relaxation processes result in an energy lowering by at least 0.35 eV (3200 cm^{-1}) compared with the neutral and in a shift of the outermost electron density from the oxygen lone pair region toward the central C−C bond and the methyl group (Figure 11). This charge migration exacerbates the nodal characteristics which characterize the anomeric interactions in the highest occupied molecular orbital and explains therefore the very strong enhancement of the related electron momentum density at $p \rightarrow 0.0$ and ∼1.05 au compared with the neutral configuration at $\alpha = 90°$. Since the ionized orbital is an oxygen lone pair, this displacement of the electron density away from the oxygen atom may at first glance seem counterintuitive. Examination of the differences of the NBO atomic charges reported in Table 2 shows that immediately after a vertical ionization event on the trans conformer, the created electron hole is merely localized on the oxygen atom and on the vicinal C_2-H_8 and C_2-H_9 bonds. After relaxation of the molecular structure of the radical cation, the hole very significantly delocalizes onto the C_1 atom in the methyl group, reflecting thereby a displacement of the total electron density toward the oxygen atom. In straightforward analogy with studies of orbital displacements in model hydrogen chains placed under electric fields of increasing strength,[52] indicating a counterfield polarization of the HOMO, the changes that the HOMO undergoes under ionization and stretching of the C_1-C_2 bond in ethanol are the results of "push−pull effects" and an avoided crossing in order to minimize exchange repulsions (Fermi correlation) with the other occupied molecular orbitals.

Examination of the results (Figure 12) of BOMD calculations at 0 K on the B3LYP/aug-cc-pVDZ potential energy surface of ethanol$^+$ at starting values of α ranging from 0 to 180° in steps of 5° beautifully confirms these predictions (in these calculations, the starting value of θ has been systematically set equal to 0°). In our simulations, the starting kinetic energy is set equal to 0, and it is therefore easy to understand from symmetry considerations, and by virtue of Helmann−Feynman theorem, that no change in the torsional characteristics is expected to arise if both α and θ are originally set equal to 0° (C_s symmetry). When the initial value of α slightly differs from 0°, significant stretchings and shortenings of the C−C and C−O bonds are delayed until the hydroxyl rotation angle α collapses to values around 90°. In contrast, extremely strong oscillations in the C−C and C−O bond lengths start immediately after ionization, with periods on the order of 40 and 100 fs, respectively, when the initial configuration for the radical cation is characterized by a α torsion angle ranging from ∼60 to ∼120°. In this case, we also note strong oscillations of the α torsion angle, from 0 to 120°, with periods on the order of ∼100 fs. Note that the adiabatic configuration [$R(C_1-C_2) = 1.76$ Å] is reached after an extremely short time interval of ∼13 fs, when the initial configuration exhibits an α torsion angle equal to 90°. In view of the energy scales of Figures 3a and 9a, it may be assumed that steeper energy gradients, and thus faster nuclear dynamics, are to be expected upon quantitative improvements of the underlying conformational energy maps. Whatever the quality of the underlying potential energy surface, these BOMD calculations confirm already the statement that strong deviations from energy minima due to thermal motions in the electronic ground state represent an important prerequisite for ultrafast nuclear dynamical motions in the final ionized state, which are, in turn susceptible, to yield significant fingerprints in the outermost electron momentum density of ethanol. Considering that a stretching of the C_1-C_2 bond by ∼0.25 Å in 13 fs only enables an increase of the outermost electron momentum distribution at $p \rightarrow 0$ au by ∼70%, compared with the results obtained for the neutral ($\alpha = 90°$, $\theta = 0°$) configuration (Figure 7), we may grossly infer from the computed trajectories that a stretching of the C_1-C_2 bond by ∼0.10 Å over an effective time scale of ∼8 fs only could bring the missing 33% of relative ionization intensity in Figure 1, and enable thereby a more quantitative match between theory and experiment.

In practice, due to the lack of energy resolution (0.6 eV) in EMS experiments at the ionization threshold, there will always be huge excesses in energies, in the form of vibrations, which will quickly convert into dissociation energies. In line with evidence from mass spectrometry measurements[53,54] and the structural consequences of the removal of an electron from the HOMO, one of the most likely reaction channels pertains to dissociation of the ethanol radical cation, $(CH_3\cdots CH_2OH)^{+\bullet}$, into a methyl radical ($CH_3^\bullet$) and a protonated form of formaldehyde ($H_2C{=}O{-}H^+$). Starting from the energy minimum on the potential energy surface of the radical cation, at $R(C_1-C_2) = 1.76$ Å, we investigate in Figure 13 the evolution of the HOMO under further stretching of the C_1-C_2 bond, up to the transition region[54] at $\sim R(C_1-C_2) = 5.26$ Å, corresponding to an energy barrier on the order of 18.2 kcal/mol relative to the energy minimum, on the path leading to the dissociation products. From this figure, it is immediately apparent that the displacement of the outermost electron densities toward the C−C bond and methyl group, which the rise of experimental (e, 2e) ionization intensities at $p \rightarrow 0$ most certainly reflects, corresponds to the very first stages of the charge (electron) transfer from the oxygen lone pair to the central C−C bond and to the methyl group, which the breaking of the C_1-C_2 bond induces. Up to very large C_1-C_2 distances, the HOMO remains partly delocalized on the C_2 and O_3 atoms, which indicates the formation of a weakly bonded charge-transfer complex through a residual interaction of the HOMO (C_{2p}) orbital of an almost planar methyl fragment with the π^* orbital of the $H_2C{=}O{-}H^+$ fragment. Examination of the atomic charges and bond orders reported in Tables 3−5 provides full support to this interpretation. Note indeed in particular that the most abrupt changes in charge occur at the level of the C_2 atom (Table 3) and that even at $R(C_1-C_2) = 5.26$ Å, the total charges of the individual

TABLE 2: NBO Analysis of Atomic Charges at the B3LYP/aug-cc-pVTZ (or B3LYP/aug-cc-pVDZ) Level

atom	neutral (gauche)	neutral (trans)	cation (vertical)[a]	ΔQ (vertical)[b]	cation (adiabatic)[c]	ΔQ (adiabatic)[d]
C_1	−0.62489 (−0.67625)	−0.61129 (−0.66585)	−0.63422 (−0.68188)	−0.02293 (−0.01603)	−0.39527 (−0.46027)	**0.21602 (0.20558)**
C_2	−0.05927 (−0.08048)	−0.05997 (−0.07851)	−0.14043 (−0.13052)	−0.08046 (−0.05201)	0.01799 (−0.00233)	0.07796 (0.07618)
O_3	−0.71605 (−0.76805)	−0.72291 (−0.77557)	−0.20197 (−0.25787)	**0.52094 (0.51770)**	−0.38259 (−0.42870)	**0.34032 (0.34687)**
H_4	0.45153 (0.47316)	0.45843 (0.47924)	0.50823 (0.52973)	0.04980 (0.05049)	0.51884 (0.54231)	0.06041 (0.06307)
H_5	0.20953 (0.22637)	0.20441 (0.22421)	0.25985 (0.27872)	0.05544 (0.05451)	0.25436 (0.27473)	0.04995 (0.05052)
H_6	0.19857 (0.21432)	0.21030 (0.22749)	0.27363 (0.28900)	0.06333 (0.06151)	0.23677 (0.25847)	0.02647 (0.03098)
H_7	0.20943 (0.22793)	0.21030 (0.22749)	0.27363 (0.28900)	0.06333 (0.06151)	0.24405 (0.26685)	0.03375 (0.03936)
H_8	0.15282 (0.18013)	0.15536 (0.18076)	0.33063 (0.34191)	**0.17527 (0.16115)**	0.24205 (0.26300)	0.08669 (0.08224)
H_9	0.17833 (0.20288)	0.15536 (0.18076)	0.33063 (0.34191)	**0.17527 (0.16115)**	0.26381 (0.28594)	0.10845 (0.10518)

[a] Results obtained upon the geometry of the neutral in its trans (C_s) conformation. [b] ΔQ (vertical) = Q[cation(vertical)] − Q[neutral (trans conformer)]. [c] Relaxed geometry. [d] ΔQ (adiabatic) = Q[cation(relaxed geometry)] − Q[neutral (trans)].

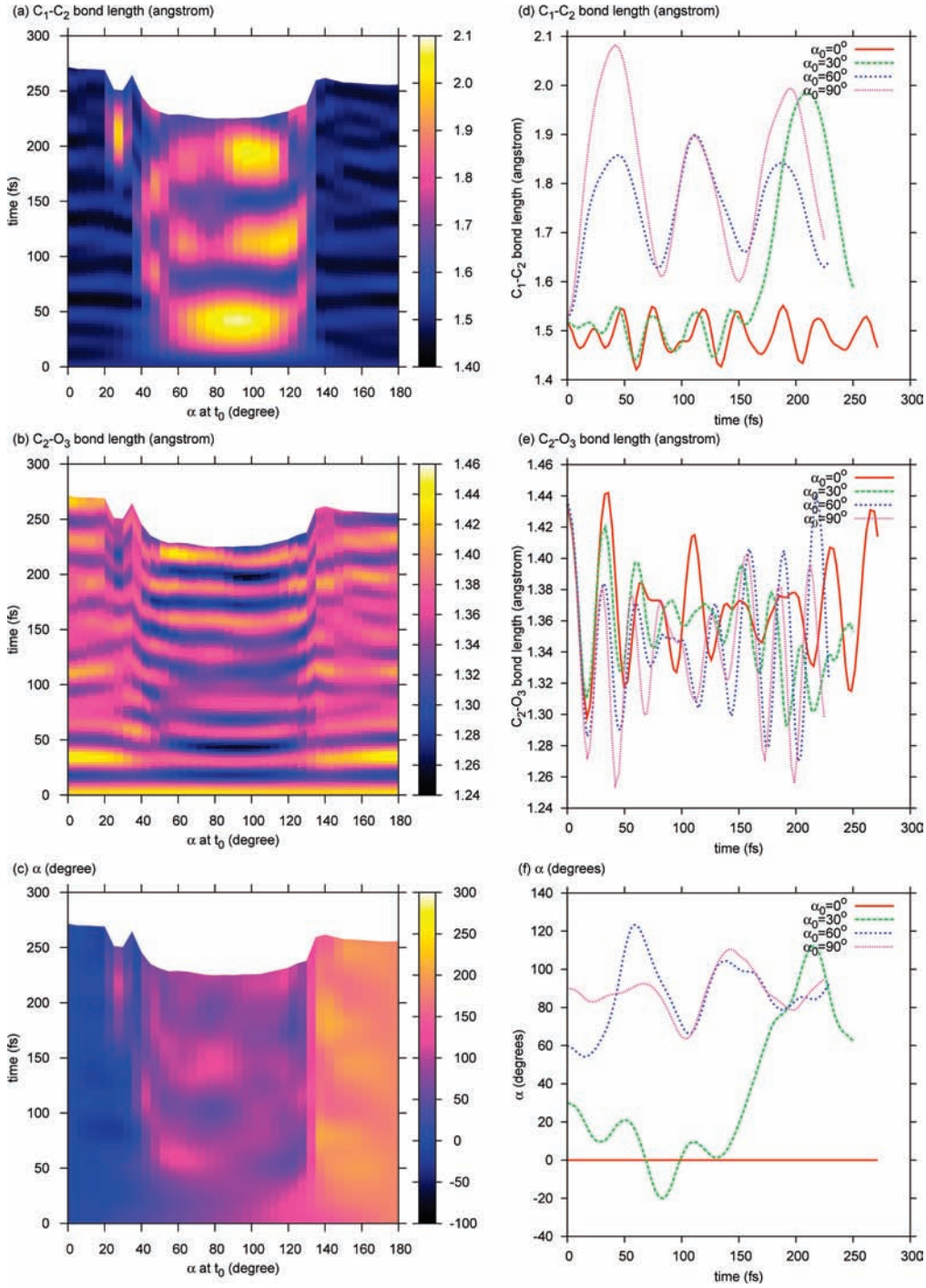

Figure 12. Time evolution of the main structural characteristics of ethanol as a function of the initial α (hydroxyl) rotation angle, according to an analysis of BOMD trajectories (B3LYP/aug-cc-pVDZ results).

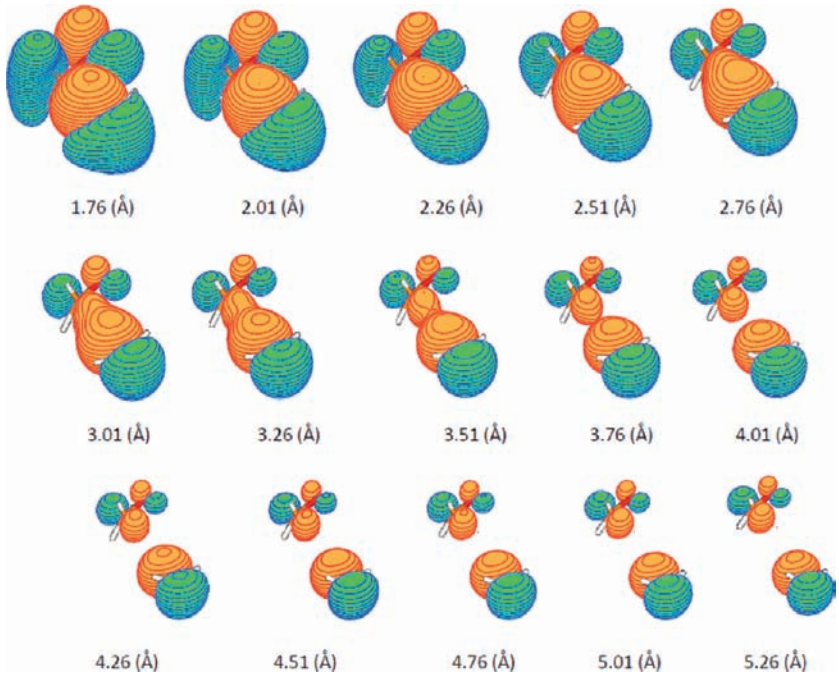

Figure 13. Evolution of the singly occupied molecular orbital (SOMO) of the ethanol radical cation as a function of the C_1-C_2 bond length (B3LYP/aug-cc-pVDZ results).

TABLE 3: NBO Study, at the B3LYP/aug-cc-pVDZ Level, of the Evolution of Atomic Charges of the Ethanol Radical Cation During the Dissociation into a Methyl Radical and $[H_2C{=}O{-}H]^+$

	atomic charges			
	Neutral			
C_1-C_2 bond length (in Å)	C_1	C_2	O_3	H_4
1.52[a]	−0.67625	−0.08048	−0.76805	0.47316
1.51[b]	−0.66585	−0.07851	−0.77557	0.47924
	Cation			
1.76	−0.46954	−0.00955	−0.42817	0.54269
2.01	−0.38789	0.08093	−0.51339	0.54236
2.26	−0.36445	0.15770	−0.54242	0.54442
2.51	−0.36802	0.21341	−0.54555	0.54723
2.76	−0.37747	0.25191	−0.54196	0.54978
3.01	−0.38529	0.27815	−0.53816	0.55175
3.26	−0.38953	0.29571	−0.53549	0.55313
3.51	−0.39018	0.30687	−0.53388	0.55403
3.76	−0.38759	0.31323	−0.53313	0.55444
4.01	−0.38295	0.31659	−0.53327	0.55466
4.26	−0.37668	0.31738	−0.53400	0.55455
4.51	−0.36976	0.31663	−0.53478	0.55424
4.76	−0.36288	0.31489	−0.53586	0.55387
5.01	−0.35637	0.31261	−0.53688	0.55351
5.26	−0.35037	0.31004	−0.53795	0.55309
∞[c]	−0.53258	0.43805	−0.49508	0.57141

[a] Gauche conformer (B3LYP/aug-cc-pVTZ geometry). [b] Trans conformer (B3LYP/aug-cc-pVTZ geometry). [c] Results from separate B3LYP/aug-cc-pVDZ calculations upon $CH_3^{\bullet}$ and CH_2OH^+.

TABLE 4: NBO Study, at the B3LYP/aug-cc-pVDZ Level, of the Evolution of Total Electric Charges of Molecular Fragments during the Dissociation of the Ethanol Radical Cation into a Methyl Radical and $[H_2C{=}O{-}H]^+$

	electric charge	
C_1-C_2 bond length (Å)	$CH_3^{\bullet}$	CH_2OH^+
1.76	0.33973	0.66027
2.01	0.36956	0.63044
2.26	0.34407	0.65593
2.51	0.30268	0.69731
2.76	0.26656	0.73344
3.01	0.24019	0.75980
3.26	0.22251	0.77748
3.51	0.21181	0.78820
3.76	0.20667	0.79333
4.01	0.20543	0.79457
4.26	0.20735	0.79265
4.51	0.21112	0.78888
4.76	0.21588	0.78412
5.01	0.22111	0.77888
5.26	0.22635	0.77364
∞	0	1

fragment are still far from convergence to the expected values at infinite distance (Table 4). Also, at $R(C_1-C_2) = 5.26$ Å, there is still a residual bond of order 0.13 between the C_1 and C_2 atoms, whereas the very substantial increase of the bond order between atoms C_2 and O_3 is consistent with the formation of a double bond and, therefore, a consequent shortening of the C_2-O_3 bond from 1.34 to 1.27 Å (Table 5).

Conclusions and Outlook to the Future

An extensive study of the influence of the molecular conformation on the valence (e, 2e) electron momentum distributions of ethanol is presented in order to interpret results obtained for this compound by means of electron momentum spectroscopy (EMS). In a first model, we focus on energy minimum forms using weight coefficients derived from thermostatistical calculations that account for the influence of hindered rotations. The analysis is based on calculations of valence one-electron and two-hole/one-particle shakeup ionization energies and of the related Dyson orbitals using one-particle Green's function theory in conjunction with the benchmark third-order algebraic diagrammatic construction scheme. Thermally and spherically averaged Dyson orbital momentum distributions are computed for all resolvable bands in the (e, 2e) ionization spectra at an impact energy of 1.2 keV. This first analysis enables overall quantitative insights into experiment and reveals a tremendously strong influence of the molecular conformation on several valence ionization bands and electron momentum distributions. Nonetheless, despite the high order

TABLE 5: NBO Study, at the B3LYP/aug-cc-pVDZ Level, of the Evolution of Wiberg Bond Indices during the Dissociation of the Ethanol Radical Cation into a Methyl Radical and $[H_2C{=}O{-}H]^+$

	Wiberg indices[b]		
	Neutral		
$C_1{-}C_2$ ($C_2{-}O_3$) bond length (Å)[a]	$C_1{-}C_2$	$C_2{-}O_3$	$O_3{-}H_4$
1.52 (1.43)[b]	1.0331	0.9290	0.7603
1.51 (1.43)[c]	1.0368	0.9222	0.7594
		Cation	
1.76 (1.34)	0.6171	1.1476	0.6859
2.01 (1.31)	0.4302	1.2408	0.6849
2.26 (1.30)	0.3062	1.3117	0.6817
2.51 (1.28)	0.2312	1.3621	0.6780
2.76 (1.28)	0.1870	1.3958	0.6748
3.01 (1.27)	0.1606	1.4178	0.6724
3.26 (1.27)	0.1449	1.4316	0.6707
3.51 (1.27)	0.1357	1.4399	0.6696
3.76 (1.27)	0.1309	1.4440	0.6691
4.01 (1.27)	0.1289	1.4450	0.6689
4.26 (1.27)	0.1289	1.4435	0.6690
4.51 (1.27)	0.1299	1.4407	0.6695
4.76 (1.27)	0.1316	1.4372	0.6699
5.01 (1.27)	0.1335	1.4335	0.6704
5.26 (1.27)	0.1354	1.4297	0.6710

[a] Geometry optimization at the B3LYP/aug-cc-pVDZ level, under the constraint of fixed $C_1{-}C_2$ bond lengths. [b] Gauche conformer (B3LYP/aug-cc-pVTZ geometry). [c] Trans conformer (B3LYP/aug-cc-pVTZ geometry).

attained in the treatment of electron correlation and relaxation, this first model fails in quantitatively reproducing the experimental momentum distribution characterizing the highest occupied molecular orbital of ethanol. The extremely limited dependence of the momentum distributions on the energy of the impinging electron rules out for all ionization bands distorted wave effects and the possibility of a breakdown of the plane wave impulse approximation. Considering the flatness of the conformational energy map of the molecular target or the rather strongly localized (oxygen lone pair) nature of the HOMO, the main purpose of the present work was to assess whether this discrepancy can be the consequence of conformational disorder in the ground state, that is, strong departures from the energy minima due to temperature effects and internal molecular motions, or nuclear dynamics in the final state, in the form of strong and fast structural relaxation effects.

Thermal averaging of the outermost momentum distributions over large sets of model structures on the potential energy surface of ethanol in its neutral ground state and further DFT calculations for the radical cation employing Born−Oppenheimer molecular dynamics demonstrate that both aspects of nuclear dynamics need to be considered for reconciling theory and experiment. The very strong broadening of the conformer distributions in the neutral ground state and the presence thereby at room temperature of a significant fraction of nuclear configurations with a hydroxyl group rotated at $\alpha \sim 90°$ appear indeed to be essential prerequisites for immediate and fast structural relaxation processes in the ionized state, which were found, in turn, to yield a tremendous increase of the outermost electron momentum distribution at vanishing electron momenta due to highly significant alterations of anomeric interactions. When the hydroxyl group is optimally oriented in the neutral ground state, the BOMD calculations demonstrate that the ionized adiabatic configuration, characterized by a stretching of the C−C bond by ∼0.25 Å and a shortening of the C−O bond by ∼0.10 Å, can be reached within a time interval of 13 fs after a sudden electron removal. This ultrafast reorganization of the molecular structure induces, in turn, a delocalization of the outermost oxygen lone pair onto the C−C bond and methyl group, which most certainly explains the rather strong experimental turn-up of the momentum distribution characterizing the HOMO of ethanol at low electron momenta. A population analysis employing natural bond orbitals shows that this turn-up may be seen as an experimental orbital fingerprint of the charge transfers resulting at the first stages of a fragmentation process, within an empirically inferred time scale on the order of 8 fs, namely, the dissociation of the ethanol radical cation ($[CH_3{-}CH_2{-}OH]^{+\bullet}$) into a methyl radical ($CH_3^{\bullet}$) and a protonated form of formaldehyde ($H_2C{=}O{-}H^+$).

An important limitation of our work is that, in view of the ultrafast nature of the investigated nuclear relaxation process, which approaches the time scale characterizing electron wave packet dynamics for charge migration processes that are driven solely by electron correlation immediately after localized ionization,[55,56] it is quite likely that the Born−Oppenheimer approximation breaks down. According to latest results by Lünnemann et al. for charge migrations in between the donor−acceptor sites of 2-phenylethyl-*N*,*N*-dimethylamine and derivative compounds,[56] we may expect that a coupling of the electronic and nuclear motions will speed up the dynamics of the relaxation processes in the final state compared with has been inferred in the present work from "clamped nuclei" configurations in the field of averaged electronic distributions. Lacking reliable experimental information on the "effective" time scale of (e, 2e) ionization processes, quantitative insights into EMS experiments on ethanol will therefore be only amenable by taking time explicitly into account in the calculations of spherically averaged (e, 2e) ionization cross sections on the grounds of quantum mechanical treatments of coupled electron−nuclear dynamics.[57,58] Because of the highly floppy nature of ethanol, which implies that extremely large sets of trajectories should be computed, this goal will probably remain beyond reach for quite a while.

Acknowledgment. All calculations presented in this work have been performed on Compaq ES45 and ES47 workstations at Hasselt University, Belgium. This work has been supported by the FWO-Vlaanderen, the Flemish branch of the Belgian National Science Foundation, and by the Bijzonder Onderzoeksfonds (BOF: special research fund) at Hasselt University. F.M. acknowledges the "Bijzonder Onderzoeksfond" of the Hasselt University for his Ph.D. fellowship. B.H. acknowledges financial support for his visiting postdoctoral fellowships from the FWO research community "Quantum chemistry: Applied and Fundamental Aspects of Density Functional Theory". B.H. wishes to thank Prof. Frank De Proft for his support and for his hospitality at the Vrije Universiteit Brussel.

References and Notes

(1) (a) McCarthy, I. E.; Weigold, E. *Phys. Rep.* **1976**, *27*, 275. (b) McCarthy, I. E.; Weigold, E. *Rep. Prog. Phys.* **1988**, *51*, 299. (c) Leung, K. T. In *Molecular Spectroscopy, electronic structure and intermolecular interactions*; Maksic, Z. B., Ed.; Springer: Berlin, Germany, 1991; p 339. (d) McCarthy, I. E.; Weigold, E. *Rep. Prog. Phys.* **1991**, *54*, 789. (e) Coplan, M. A.; Moore, J. H.; Doering, J. P. *Rev. Mod. Phys.* **1994**, *66*, 985. (f) McCarthy, I. E.; Weigold, E. *Electron Momentum Spectroscopy*; Kluwer Academic, Plenum: New York, 1999. (g) Lahman-Bennami, A. *J. Electron Spectrosc. Relat. Phenom.* **2002**, *123*, 365.

(2) (a) Zheng, Y.; Neville, J. J.; Brion, C. E. *Science* **1995**, *270*, 5237. (b) Neville, J. J.; Zheng, Y.; Brion, C. E. *J. Am. Chem. Soc.* **1996**, *118*, 10533.

(3) Neville, J. J.; Zheng, Y.; Hollebone, B. P.; Cann, N. M.; Brion, C. E.; Kim, C.-K.; Wolfe, S. *Can. J. Phys.* **1996**, *74*, 773.

(4) Huang, Y. R.; Knippenberg, S.; Hajgató, B.; Francois, J.-P.; Deng, J. K.; Deleuze, M. S. *J. Phys. Chem. A* **2007**, *111*, 5879.

(5) (a) Pang, W.; Shang, R.; Gao, J.; Gao, N.; Chen, X. J.; Deleuze, M. S. *Chem. Phys. Lett.* **1998**, *296*, 605. (b) Pang, W. N.; Gao, J. F.; Ruan, C. J.; Shang, R. C.; Trofimov, A. B.; Deleuze, M. S. *J. Chem. Phys.* **2000**, *112*, 8043.

(6) Deleuze, M. S.; Wang, W. N.; Salam, A.; Shang, R. C. *J. Am. Chem. Soc.* **2001**, *123*, 4049.

(7) Deleuze, M. S.; S. Knippenberg, S. *J. Chem. Phys.* **2006**, *124*, 104309.

(8) Wu, F.; Chen, X. J.; Shan, X.; Tian, S. X.; Li, Z. J.; Xu, K. Z. *J. Phys. Chem. A* **2008**, *112*, 4360.

(9) (a) Yang, T. C.; Su, G. L.; Ning, C. G.; Deng, J. K.; Wang, F.; Zhang, S. F.; Ren, X. G.; Huang, Y. R. *J. Phys. Chem. A* **2007**, *111*, 4927. (b) Ning, C. G.; Huang, Y. R.; Zhang, S. F.; Deng, J. K.; Liu, K.; Luo, Z. H.; Wang, F. *J. Phys. Chem. A* **2008**, *112*, 11078.

(10) Xue, X. X.; Yan., M; Wu., F.; Shan, X.; Xu., K. Z.; Chen, X. J. *Chin. J. Chem. Phys* **2008**, *21*, 515.

(11) Yan, M.; Shan, X.; Wu., F.; Xia, X.; Wang, K. D.; Xu, K. Z.; Chen, X. J. *J. Phys. Chem. A* **2009**, *113*, 507.

(12) Ning, C. G.; Luo, Z. H.; Huang, Y. R.; Hajgató, B.; Morini, F.; Liu, K.; Zhang, S. F.; Deng, J. K.; Deleuze, M. S. *J. Phys. B* **2008**, *41*, 175103.

(13) Morini, F.; Hajgató, B.; Deleuze, M. S.; Ning, C. G.; Deng, J. K. *J. Phys. Chem. A* **2008**, *112*, 9083.

(14) Schwarz, W. H. E. *Angew. Chem.* **2006**, *45*, 1508.

(15) (a) Pickup, B. T. *Chem. Phys.* **1977**, *19*, 193. (b) Öhrn, Y.; Born, G. *Adv. Quantum Chem.* **1981**, *13*, 1. (c) McWeeny, R.; Pickup, B. T. *Rep. Prog. Phys.* **1980**, *43*, 1065. (d) Deleuze, M.; Pickup, B. T.; Delhalle, J. *Mol. Phys.* **1994**, *83*, 655. (e) Seabra, G. M.; Kaplan, I. G.; Zakrzewski, V. G.; Ortiz, J. V. *J. Chem. Phys.* **2004**, *121*, 4142. (f) Oana, C. M.; Krylov, A. I. *J. Chem. Phys.* **2007**, *127*, 234106.

(16) (a) Duffy, P.; Chong, D. P.; Casida, M. E.; Salahub, D. R. *Phys. Rev. A* **1994**, *50*, 4704. (b) Hollebone, B. P.; Neville, J. J.; Zheng, Y.; Brion, C. E.; Wang, Y.; Davidson, E. R. *Chem. Phys.* **1995**, *196*, 13. (c) Rolke, J.; Cann, N.; Zheng, Y.; Hollebone, B. P.; Brion, C. E.; Wang, Y. A.; Davidson, E. R. *Chem. Phys.* **1995**, *201*, 1. (d) Duffy, P. *Can. J. Phys.* **1996**, *74*, 763. (e) Rolke, J.; Brion, C. E. *Chem. Phys.* **1996**, *173*, 206. (f) Fan, X. W.; Chen, X. J.; Zhou, S. J.; Zheng, Y.; Brion, C. E.; Frey, R.; Davidson, E. R. *Chem. Phys. Lett.* **1997**, *276*, 346.

(17) (a) Ning, C. G.; Ren, X. G.; Deng, J. K.; Su, G. L.; Zhang, S. F.; Knippenberg, S.; Deleuze, M. S. *Chem. Phys. Lett.* **2006**, *421*, 52. (b) Ning, C. G.; Hajgató, B.; Huang, Y. R.; Zhang, S. F.; Liu, K.; Luo, Z. H.; Knippenberg, S.; Deng, J. K.; Deleuze, M. S. *Chem. Phys.* **2008**, *19*, 343. (c) Huang, Y. R.; Hajgató, B.; Ning, C. G.; Zhang, S. F.; Liu, K.; Luo, Z. H.; Deng, J. K.; Deleuze, M. S. *J. Phys. Chem. A* **2008**, *112*, 2339. (d) Huang, Y. R.; Ning, C. G.; Deng, J. K.; Deleuze, M. S. *Phys. Chem. Chem. Phys.* **2008**, *10*, 2374.

(18) See, for example: Knippenberg, S.; Huang, Y. R.; Hajgato, B.; François, J.-P.; Deleuze, M. S. *J. Chem. Phys.* **2006**, *125*, 104309, and references therein.

(19) Nicholson, R. J. F.; McCarthy, I. E.; Weyrich, W. *J. Phys. B* **1999**, *32*, 3873.

(20) Landau, L. D.; Lifshitz, E. M. *Quantum Mechanics: Non-relativistic Theory*; Pergamon: Oxford, U.K., 1977.

(21) (a) Takahashi, M.; Saito, T.; Hiraka, J.; Udagawa, Y. *J. Phys. B* **2003**, *36*, 2539. (b) Takahashi, M.; Khajuria, Y.; Udagawa, Y. *Phys. Rev. A* **2003**, *68*, 042710. (c) Ren, X. G.; Ning, C. G.; Deng, J. K.; Zhang, S. F.; Su, G. L.; Huang, F.; Li, G. Q. *Phys. Rev. Lett.* **2005**, *94*, 163201. (d) Ren, X. G.; Ning, C. G.; Deng, J. K.; Su, G. L.; Zhang, S. F.; Huang, Y. R.; Li, G. Q. *Phys. Rev. A* **2005**, *72*, 042718. (e) Ning, C. G.; Ren, X. G.; Deng, J. K.; Zhang, S. F.; Su, G. L.; Huang, F.; Li, G. Q. *Chem. Phys. Lett.* **2005**, *407*, 423. (f) Ning, C. G.; Ren, X. G.; Deng, J. K.; Su, G. L.; Zhang, S. F.; Li, G. Q. *Phys. Rev. A* **2006**, *73*, 022704. (g) Miyake, Y.; Takahashi, M.; Watanabe, N.; Khajuria, Y.; Udagawa, Y.; Sakai, Y.; Mukova, T. *Phys. Chem. Chem. Phys.* **2006**, *8*, 3022. (h) Ren, X. G.; Ning, C. G.; Deng, J. K.; Zhang, S. F.; Su, G. L.; Huang, Y. R.; Li, G. Q. *J. Electron Spectrosc. Relat. Phenom.* **2006**, *151*, 92. (i) Ning, C. G.; Ren, X. G.; Deng, J. K.; Su, G. L.; Zhang, S. F.; Knippenberg, S.; Deleuze, M. S. *Chem. Phys. Lett.* **2006**, *421*, 52.

(22) Li, Z. J.; Chen, X. J.; Shan, X.; Liu, T.; Xu, K. Z. *J. Chem. Phys.* **2009**, *130*, 054302.

(23) Knippenberg, S.; Deleuze, M. S.; Cleij, T. J.; François, J.-P.; Cederbaum, L. S.; Eland, J. H. D. *J. Phys. Chem. A* **2005**, *109*, 4267.

(24) Knippenberg, S.; Nixon, K. L.; Brunger, M. J.; Maddern, T.; Campbell, L.; Trout, N.; Wang, F.; Newell, W. R.; Deleuze, M. S.; François, J.-P.; Winkler, D. A. *J. Chem. Phys.* **2004**, *121*, 10525.

(25) Cho, A. *Science* **2004**, *303*, 942.

(26) (a) Ning, C. G.; Deng, J. K.; Su, G. L.; Zhou, H.; Ren, X. G. *Rev. Sci. Instrum.* **2004**, *75*, 3062. (b) Ren, X. G.; Ning, C. G.; Deng, J. K.; Zhang, S. F.; Su, G. L.; Huang, F.; Li, G. Q. *Rev. Sci. Instrum.* **2005**, *76*, 063103.

(27) (a) Pickup, B. T.; Goscinski, O. *Mol. Phys.* **1973**, *26*, 1013. (b) Cederbaum, L. S.; Hohlneicher, G.; von Niessen, W. *Mol. Phys.* **1973**, *26*, 1405. (c) Cederbaum, L. S.; Domcke, W. *Adv. Chem. Phys.* **1977**, *36*, 205. (d) von Niessen, W.; Schirmer, J.; Cederbaum, L. S. *Comput. Phys. Rep.* **1984**, *1*, 57. (e) Ortiz, J. V. In *Computational Chemistry: Reviews of Current Trends*; Leszczynski, J., Ed.; World Scientific: Singapore, 1997; Vol. 2, p 1. (f) Linderberg, J.; Öhrn, Y. *Propagators in Quantum Chemistry*, 2nd ed.; Wiley-Interscience: New York, 2004.

(28) (a) Schirmer, J.; Cederbaum, L. S.; Walter, O. *Phys. Rev. A* **1983**, *28*, 1237. (b) von Niessen, W.; Schirmer, J.; Cederbaum, L. S. *Comput. Phys. Rep.* **1984**, *1*, 57. (c) Schirmer, J.; Angonoa, G. *J. Chem. Phys.* **1989**, *91*, 1754. (d) Weikert, H.-G.; Meyer, H.-D.; Cederbaum, L. S.; Tarantelli, F. *J. Chem. Phys.* **1996**, *104*, 7122. (e) Deleuze, M. S.; Giuffreda, M. G.; François, J.-P.; Cederbaum, L. S. *J. Chem. Phys.* **1999**, *111*, 5851. (f) Deleuze, M. S. *Int. J. Quantum Chem.* **2003**, *93*, 191.

(29) McQuarrie, D. A. *Statistical Thermodynamics*; Harper and Row: New York, 1976.

(30) Ayala, P. Y.; Schlegel, H. B. *J. Chem. Phys.* **1998**, *108*, 2314.

(31) Kahn, K.; Bruice, T. C. *Chem. Phys. Chem.* **2005**, *6*, 487.

(32) (a) Kakar, R. K.; Quade, C. R. *J. Chem. Phys.* **1980**, *72*, 4300. (b) Pearson, J. C.; Sarsty, K. V. L. N.; Herbst, E.; de Lucia, F. C. *J. Mol. Spectrosc.* **1996**, *175*, 146. (c) Shaw, R. A.; Weiser, H.; Dutler, R.; Rauk, A. *J. Am. Chem. Soc.* **1990**, *112*, 5401. (d) Abu-samba, M.; Børve, K. J. *Phys. Rev. A* **2006**, *74*, 042508.

(33) Senent, M. L.; Smeyers, Y. G.; Domingues-Gómez, R.; Villa, M. *J. Chem. Phys.* **2000**, *112*, 5809.

(34) Durig, J. R.; Larsen, R. A. *J. Mol. Struct.* **1989**, *238*, 195.

(35) (a) Fang, W. Ph.D. Thesis, Hefei National Laboratory for Physical Sciences at Microscale, Department of Modern Physics, University of Science and Technology of China, Hefei, Anhui, 230026, People's Republic of China, May 2007 (private communication by Chen, X.J.; promotor, on 28 Aug 2008). (b) Chen, X. J.; Fang, W.; Yan, M.; Li, H. B.; Tian, S. X.; Shan, X.; Wang, K.; Li, Z.; Xu, K. *Chem. Phys. Lett.* **2009**, *472*, 19.

(36) (a) Bunker, D. L. *Methods Comput. Phys.* **1971**, *10*, 287. (b) Raff, L. M.; Thompson, D. L. In *Theory of Chemical Reaction Dynamics*; BaerM., Ed.; CRC: Boca Raton, FL, 1985. (c) *Advances in Classical Trajectory Methods*; Hase, W. L., Ed.; JAI: Stamford, CT, 1991; Vol. 1−3. (d) Thompson, D. L. In *Encyclopedia of Computational Chemistry*; Schleyer, P. v. R., Allinger, N. L., Kollman, P. A., Clark, T., Schaefer, H. F., III, Gasteiger, J., Schreiner, P. R., Eds.; Wiley: Chichester, U.K., 1998; p 3506. (e) Helgaker, T.; Uggerud, E.; Jensen, H. J. A. *Chem. Phys. Lett.* **1990**, *173*, 145. (f) Uggerud, E.; Helgaker, T. *J. Am. Chem. Soc.* **1992**, *114*, 4265. (g) Chen, W.; Hase, W. L.; Schlegel, H. B. *Chem. Phys. Lett.* **1994**, *228*, 436. (h) Millam, J. M.; Bakken, V.; Chen, W.; Hase, W. L.; Schlegel, H. B. *J. Chem. Phys.* **1999**, *111*, 3800. (i) Li, X.; Millam, J. M.; Schlegel, H. B. *J. Chem. Phys.* **2000**, *113*, 10062. (j) Bolton, K.; Hase, W. L.; Peshlherbe, G. H. In *Modern Methods for Multidimensional Dynamics Computation in Chemistry*; Thompson, D. L., Ed.; World Scientific: Singapore, 1998; p 143. (k) Hase, W. L.; Duchovic, R. J.; Hu, X.; Komornicki, A.; Lim, K. F.; Lu, D.-H.; Peslherbe, G. H.; Swamy, K. N.; Linde, S. R. V.; Varandas, A.; Wang, H.; Wolfe, R. J. *Quantum Chem. Program Exchange* **1996**, *16*, 671.

(37) Parr, R. G.; Yang, W. *Density Functional Theory of Atoms and Molecules*; Oxford University Press: New York, 1989.

(38) (a) Becke, A. D. *J. Chem. Phys.* **1993**, *98*, 5648. (b) Lee, C.; Yang, W.; Parr, R. G. *Phys. Rev.B* **1988**, *37*, 785.

(39) (a) Dunning, T. H., Jr. *J. Chem. Phys.* **1989**, *90*, 1007. (b) Kendall, R. A.; Dunning, T. H.; Harrison, R. J. *J. Chem. Phys.* **1992**, *96*, 6796. (c) Woon, D. E.; Dunning, T. H., Jr. *J. Chem. Phys.* **1994**, *100*, 2975. (d) Peterson, K. A.; Woon, D. E.; Dunning, T. H., Jr. *J. Chem. Phys.* **1994**, *100*, 7410.

(40) Duffy, P.; Casida, M. E.; Brion, C. E.; Chong, D. P. *Chem. Phys.* **1992**, *159*, 347.

(41) (a) Bulirsch, R.; Stoer, J. In *Introduction to Numerical Analysis*; Springer-Verlag: New York, 1991. (b) Press, W. H.; Flannery, B. P.; Teukolsky, S. A.; Vetterling, W. T. Richardson Extrapolation and the Bulirsch-Stoer Method. *Numerical Recipes in FORTRAN: The Art of Scientific Computing*, 2nd ed.; Cambridge University Press: Cambridge, U.K., 1992; pp 718−725.

(42) Wiberg, K. B. *Tetrahedron* **1968**, *24*, 1083.

(43) (a) Foster, J. P.; Weinhold, F. *J. Am. Chem. Soc.* **1980**, *102*, 7211. (b) Reed, A. E.; Curtiss, L. A.; Weinhold, F. *Chem. Rev.* **1988**, *88*, 899. (c) Weinhold, F.; Landis, C. R. *Chemistry Education: Research and Practice in Europe*, special Structural Concepts issue; 2001; Vol. 2, pp 91−104.

(44) Bridgeman, A. J.; Cavigliasso, G.; Ireland, L. R.; Rotery, J. *J. Chem. Soc., Dalton Trans.* **2001**, 2095.

(45) Shundalov, M. B.; Romanov, O. G. *J. Appl. Spectrosc.* **2008**, *75*, 360.

(46) Chun, F. S.; Richard Quade, C. *J. Mol. Spectrosc.* **2000**, *199*, 34.

(47) Dyczmons, V. *J. Phys. Chem. A* **2004**, *108*, 2080.

(48) Shi, Y. J.; Consta, S; Bas, A. K.; Mallik, B.; Lacey, D.; Lipson, R. H. *J. Chem. Phys.* **2002**, *116*, 6990.

(49) (a) Bellville, D. J.; Bauld, N. L. *J. Am. Chem. Soc.* **1982**, *104*, 5700. (b) Yates, W. J.; Bouma, W. J.; Radom, L. *Tetrahedron* **1986**, *42*, 6225. (c) George, M.; Kingsmill, C. A.; Suh, D.; Terlouw, J. K.; Holmes, J. L. *J. Am. Chem. Soc.* **1994**, *116*, 7807. (d) Brenner, V.; Milliet, A.; Mourgues, P.; Ohanessian, G.; Audier, H. E. *J. Phys. Chem.* **1995**, *99*, 10837.

(50) Gauld, J. W.; Radom, L. *Chem. Phys. Lett.* **1997**, *275*, 28.

(51) Deng, J. K.; Li, G. Q.; Huang, J. D.; Deng, H.; Wang, X. D.; Wang, F.; He, Y.; Zhang, Y. A.; Ning, C. G.; Gao, N. F.; Wang, Y.; Chen, X. J.; Zheng, Y.; Brion, C. E. *Chem. Phys. Lett.* **1999**, *313*, 134.

(52) Deleuze, M.; Delhalle, J.; Pickup, B. T. *Theor. Chim. Acta* **1992**, *82*, 309.

(53) (a) Sharma, V.; Bapat, B. *J. Chem. Phys.* **2006**, *125*, 044305. (b) Griffin, L. L.; Trager, J. C.; Hudson, C. E.; McAdoo, D. J. *Int. J. Mass Spectrom.* **2002**, *217*, 23.

(54) Lu, H.-F.; Li, F.-Y.; Nagaya, K.; Hayashi, M.; Mishima, K.; Lin, S. H. *J. Mol. Struct.: THEOCHEM* **2006**, *761*, 159.

(55) (a) Cederbaum, L. S.; Zobeley, J. *Chem. Phys. Lett.* **1999**, *307*, 205. (b) Breidbach, J.; Cederbaum, L. S. *J. Chem. Phys.* **2003**, *118*, 3983. (c) Kuleff, A. I.; Breidbach, J.; Cederbaum, L. S. *J. Chem. Phys.* **2005**, *123*, 044111. (d) Henning, H.; Breidbach, J.; Cederbaum, L. S. *J. Phys. Chem. A* **2005**, *109*, 409. (e) Breidbach, J.; Cederbaum, L. S. *J. Chem. Phys.* **2007**, *126*, 034101.

(56) (a) Lünnemann, S.; Kuleff, A. I.; Cederbaum, L. S. *Chem. Phys. Lett.* **2008**, *450*, 232. (b) Lünnemann, S.; Kuleff, A. I.; Cederbaum, L. S. *J. Chem. Phys.* **2008**, *129*, 104305.

(57) (a) Deumens, E.; Diz, A.; Longo, R.; Öhrn, Y. *Rev. Mod. Phys.* **1994**, *66*, 917. (b) Chelkovwski, S.; Zuo, T.; Atabek, O.; Bandrauk, A. D. *Phys. Rev. A* **1995**, *52*, 2977. (c) Morales, J.; Diz, A.; Deumens, E.; Öhrn, Y. *J. Chem. Phys.* **1995**, *103*, 9968. (d) Jacquemin, D.; Morales, J. A.; Deumens, E.; Öhrn, Y. *J. Chem. Phys.* **1997**, *107*, 6146. (e) Broeckhove, J.; Coutinho-Neto, M. D.; Deumens, E.; Öhrn, Y. *Phys. Rev. A* **1997**, *56*, 4996. (f) Hedström, M.; Morales, J. A.; Deumens, E.; Öhrn, Y. *Chem. Phys. Lett.* **1997**, *279*, 241. (g) Deumens, E.; Öhrn, Y. *J. Phys. Chem. A* **2001**, *105*, 2660. (h) Öhrn, Y.; Deumens, E. *Adv. Chem. Phys.* **2002**, *124*, 323. (i) Cabrera-Trujillo, R.; Sabin, J. R.; Deumens, E.; Öhrn, Y. *Adv. Quantum Chem.* **2004**, *47*, 251. (j) Stolterfoht, N.; Hellhammer, R.; Pesic, Z.; Cabrera-Trujillo, R.; Deumens, E.; Öhrn, Y.; Sabin, J. R. *Adv. Quantum Chem.* **2007**, *52*, 149.

(58) Cederbaum, L. S. *J. Chem. Phys.* **2008**, *128*, 124101.

JP9027029